Project acronym:	**Geo-Drill**		
Project title:	Development of novel and cost-effective drilling technology for geothermal Systems		
Activity:	LCE-07-17-Renewables		
Call:	H2020-LC-SC3-2018-RES-TwoStages		
Funding Scheme:	RIA	**Grant Agreement No:**	815319
WP 2	**Development of Materials and Coatings**		

D2.4 - Report on Drill bit tooth, fluidic oscillator and stabilizer coating manufacture and properties

Due date:	30/09/2020(M18)	
Actual Submission Date:	03/02/2021	
Lead Beneficiary:	TWI	
Main authors/contributors:	TWI	
Dissemination Level[1]:	PU	
Nature:	REPORT	
Status of this version:		**Draft under Development**
		For Review .by Coordinator
	X	**Submitted**
Version:	1.0	
Abstract	The deliverable reports on performed to develop coating systems using the high-velocity oxygen fuel (HVOF) process, including tungsten carbide (WC) coatings, chromium carbide (CrC) coatings, self-fluxing alloy (NiCrFeSiB) coatings, and nano-crystalline/amorphous coatings.	

REVISION HISTORY

Version	Date	Main Authors/Contributors	Description of changes
V1	29/01/2021	TWI	

[1] Dissemination level security:

PU – Public (e.g. on website, for publication etc.) / **PP** – Restricted to other programme participants (incl. Commission services) / **RE** – Restricted to a group specified by the consortium (incl. Commission services) / **CO** – confidential, only for members of the consortium (incl. Commission services)

This project has received funding from the *European Union's Horizon 2020 research and innovation programme* under grant agreement No 818576

This project has received funding from the European Union's Horizon 2020 program Grant Agreement No 815319. This publication reflects the views only of the author(s), and the Commission cannot be held responsible for any use which may be made of the information contained therein.

Summary

This deliverable describes work that was performed to develop coating systems using the high-velocity oxygen fuel (HVOF) process, including tungsten carbide (WC) coatings, chromium carbide (CrC) coatings, self-fluxing alloy (NiCrFeSiB) coatings, and nano-crystalline/amorphous coatings.

Design of experiments (DoE) was used for process development of each coating system. The best coating from each material type was selected to be tested further in WP3. The down-selection was determined by comparing surface roughness, microstructure, deposition efficiency, porosity, hardness and adhesion strength of the coatings.

The selected coatings were then produced on the substrates as required for WP3 testing, to be ranked for suitability for geodrillng applications. Detailed information on the selection of these substrates has been reported in PR1 (M18) report.

Objectives Met

The work described contributes to the following WP2 objective:

- To synthesise materials, coatings and develop coating technique for Geo-Drill components.

CONTENTS

1. INTRODUCTION

1.1 Overview

Failure of drilling parts is a serious challenge in the geothermal industry, where the tools are expected to operate in extreme conditions. To address the challenge, applying coatings is believed to be the most effective solution to extend drilling tool service lifetime. In this report, we will present high velocity oxygen fuel (HVOF) process parameter development for various coating systems, including tungsten carbide (WC) coatings, chromium carbide (CrC) coatings, self-fluxing alloy (NiCrFeSiB) coatings, and nano-crystalline/amorphous coatings. Development of suitable parameters has been defined in the KPI report submitted earlier (D1.5: Geo-Drill KPIs).

1.2 High velocity oxygen fuel (HVOF) spray

High velocity oxygen fuel (HVOF) spray is a commonly used thermal spray technology and is widely used to deposit carbide-based cermets, metals and alloy coatings. It is characterised by higher velocity and lower flame temperature compared with other thermal spray processes, which offers the ability to deposit dense and good adherent coatings. Thus, it is mainly used for applying powder materials with a relatively low melting point and those that may experience thermal degradation at high temperature.

Among various HVOF systems, a liquid fuel HVOF system JP5000 is a proven design using economical kerosene fuel, offering higher particle velocities in the range of 1005-1115m/s and a more uniform distribution of particles within the spray stream [1]. Figure 1 shows a process diagram of the JP5000 system. Liquid fuel and oxygen are fed into the gun and ignited in the combustion chamber. The flame velocity increases with rising combustion chamber temperature, and is accelerated through a converging-diverging nozzle. The spatial distribution of particle density depends strongly on the carrier gas flow rate [2].

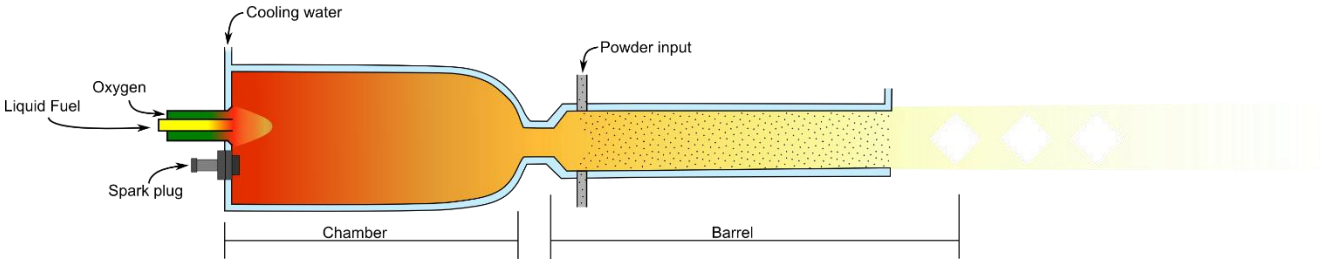

Figure 1 HVOF process diagram – JP5000

The HVOF spray process is very complex. Feedstock, spray process parameters and particle-substrate interactions all affect deposit quality and hence coating performance. Oxygen and fuel flow rates (oxygen/fuel ratio) have a direct influence on flame velocity and temperature. Other variables, which play an important role, include spray distance, spray angle etc. During spraying, particles are fully-melted or partially melted, depending on flame temperature, particle dwell time, material melting point and thermal conductivity. The control and optimisation of the HVOF process in order to achieve coatings with desired properties is a highly challenging task [3].

Substrates are generally prepared by cleaning to Sa 3 (white metal finish) in accordance with ISO 8501 and profiled by grit blasting. Coatings deposited by HVOF spraying are characterised by a mechanical bond between the coating and the substrate in the as-deposited condition.

1.3 Coating systems

1.3.1 Tungsten carbide (WC) coatings

WC coatings are well-known for their outstanding wear resistance. Many studies have confirmed that WC coatings exhibited higher hardness, fracture toughness and therefore wear-resistant performance compared with other carbides. HVOF is a well-used thermal spraying technique for WC feedstock in order to obtain excellent adhesion strength and high density. Decarburisation of WC has been reported to have a detrimental effect on the abrasive wear resistance of coating, which is caused by increasing brittleness and decrease in hard particle content [4].

For WC coatings, a ductile binder such as cobalt (Co) or nickel (Ni) is commonly used. While the carbide phase WC provides hardness and wear resistance, the ductile binder contributes to toughness and strength. The chemical bond between WC and Co results in a very low interfacial energy, nearly perfect wetting and very good adhesion in the solid state [4].

1.3.2 Chromium carbide /nickel chromium (Cr_3C_2/NiCr) coating

Among various carbide materials, WC based coatings are usually used below 500°C, while Cr_3C_2 based coatings can operate at temperatures up to 900°C. Though Cr_3C_2 based coatings offer lower hardness and lower wear resistance than WC coatings at lower temperatures, they have better performance in high temperature wear applications. Due to their high melting point, Cr_3C_2/NiCr coatings also offer superior oxidation and corrosion resistance. A Cr_3C_2 coating is normally composed of two phases; the carbide ceramic phase offers wear resistance and the binding matrix NiCr offers corrosion resistance [5].

1.3.3 Self-fluxing alloy (NiCrFeSiB) coatings

Nickel alloys containing substantial amounts of boron and silicon possesses the interesting property of 'self-fluxing'. Both additives react with oxides at high temperatures to form low melting point borosilicate, which prevents further oxidation of active elements in the alloys. Simultaneously the low melting eutectic of Ni-Ni_3B appears with the highly wettable borosilicate, and causes fusion and densification to occur at lower temperatures. The thermal input to the substrate can also be decreased [6]. Self-fluxing alloys can be metallurgically fused to the substrate during or following heat treatment when the entire coating (and often the entire substrate) is heated above the melting point of the alloy (typically around 1100° C).

1.3.4 Nanocrystalline/amorphous coatings

The development of nanocrystalline/amorphous materials has attracted significant interest in the field of new materials design. Though WC-Co-Cr HVOF sprayed coating is considered a good candidate for hard chromium coating and presents combined wear and corrosion resistance, it is an expensive coating system which limits its wider use in industry. Nanocrystalline/amorphous materials were investigated as an alternative option. The magnetic, chemical and mechanical properties of materials are largely enhanced when the grain size is of the order of nanometres. For amorphous materials, the absence of crystal structure generates macroscopic behaviour different from that of the polycrystalline state, especially mechanical and magnetic properties [7].

Among various developed nanocrystalline/amorphous materials, Fe-Cr-Mo-W-Mn-B-C-Si was designed to have high glass forming ability. Through detailed thermal analysis experiments, this alloy was found to exhibit a reduced glass temperature of 0.57, a glass transition temperature of 579°C, and a three-stage crystallisation with peaks at 630°C, 671°C and 777°C. After argon atomisation, the powder was sieved and air classified to yield feedstock powder nominally +15 to -53 µm in diameter, which had an appropriate distribution for being sprayed with the JP5000 gun system.

2. APPROACH

2.1 Materials

2.1.1 Powders

In order to achieve higher technology readiness levels (TRLs) for the drilling system developed in the project and to maintain a consistent coating quality in the geothermal environment, powders selected in this report all satisfy the following criteria:

- Commercially available;
- To offer improved abrasion resistance and lower coefficient of friction at elevated temperature (minimum 250°C);
- To offer corrosion and erosion resistant at elevated temperature (minimum 250°C);
- To enable achieving a relatively smooth surface finish.

All the powders selected for preparing various coating systems are presented in Table 1, including:

- Two WC based powders, with Woka3652 being conventional sized powder and Woka3652FC being ultrafine powder, both supplied by Oerlikon.
- Two NiCr/CrC powders, with 1375VM being conventional powder and 1375VF being finer powder, both supplied by Praxair.
- One NiCrFeSiB powder, 1660-02 from Hoganas (Table 2).
- One nanocrystalline/amorphous, SHS 7574HV from LincolnElectric.

Table 1 Selected powders with properties suggested by Suppliers.

TWI ID	Powder	Chemistry	Size, µm	Supplier	Erosion	Abrasion	Wear	Corrosion	Max temp, °C
4091	Woka 3652	WC10Co4Cr	-45+15	Oerlikon metco	Y	Y	Y	Y	500
4278	Woka 3652 FC	WC10Co4Cr	-45+15, sub	Oerlikon metco	Y	Y	Y	Y	500
3751	1375VM	NiCr 25.0, Cr_3C_2 75.0	-45+16	Praxair	Y	Y	Y	Y	781
4277	1375VF	NiCr 25.0, Cr_3C_2 75.0	-45+11	Praxair	Y	Y	Y	Y	781
4279	1660-02	NiCrFeSiB	-50+20	Hoganas	Y	-	-	Y	820
4274	SHS 7574HV	C3Cr25B5Mo20Mn5 Si2W10Fe balance	-53+20	LincolnElectric	-	Y		Y	-

Table 2 Chemical properties of powder 1660-02 (information provided by Höganäs Belgium S.A.)

Elements	C	Fe	Cr	Si	B	O	Ni
Amount, wt %	0.74	3.83	14.97	4.42	3.27	0.031	balance

2.1.2 Substrates

The selection of reference substrates is based on a preliminary study on currently used hammer parts, which was reported in detail in PR1 (M18) report. Specification and nominal compositions of selected steel substrates are given in Table 3. From the preliminary study, some steels used for drilling components present high hardness (Table 7 in PR1 M18 report). Therefore, both 440B and 835M30 test coupons were heat-treated and tempered from their annealed condition before applying coatings.

Bright mild steel substrates (40×40×6 mm) were used for all the DoE matrices. Once best parameters were selected, coating were then deposited onto the selected substrates to be tested in WP3. For all the substrates, their surface was ground flat and then grit-blasted to remove surface contaminants and to create a rough surface for better adhesion. Surface preparation parameters are described below:

- Blast media: alumina;
- Mesh size:60;
- Running air pressure:60 psi;
- Stand-off distance: 80mm;
- Abrasive nozzle: Ø=8mm ID.

The roughened surface was then cleaned using compressed air and alcohol. Coating deposition was then carried out immediately.

Table 3 Material specifications and nominal compositions of steel substrates

Steels	Composition
Bright mild steel (EN3B)	C 0.180, Si 0.160, Mn 0.770, P 0.009, S 0.007, Cr 0.060, Mo 0.040, Ni 0.080, Cu 0.012, Al 0.009, Fe bal.
34CrNiMo6 (EN24T)	C 0.430, Si 0.310, Mn 0.590, P 0.009, S 0.033, Cr 1.200, Mo 0.220, Ni 1.400, Pb 0.0007, Cu 0.200, Sn 0.014, Ca 0.0029, N 0.012, Nb 0.005, Ti 0.0048, V 0.010
440B	C 0.83, Si 0.43, Mn 0.40, P 0.029, S 0.001, Cr 0.001, Cr 16.7, Mo 0.59
835M30 (EN 30B)	C 0.310, Si 0.260, Mn 0.550, P 0.008, S 0.0047, Cr 1.190, Mo 0.330, Ni 4.100, Cu 0.150, Sn 0.008,Al 0.024, Ti 0.0014, N 0.006, Ca 0.005, V 0.003

2.2 HVOF spray process

The Tafa JP5000 HVOF system at TWI, manufactured by Praxair Surface Technologies, was used for coating deposition in the report (Figure 2). Powder was fed radially into the gun through a two-way or three-way powder feeder. Varying the barrel length of JP5000 directly changes the time the powder resides in the nozzle, allowing the degree of melting of the powder to be altered. In this work both 4 inch (102mm) and 6 inch (152mm) nozzles were used. Liquid kerosene and oxygen were supplied to the spraying gun using a Tafa 5120 control console. Powder was fed into the gun using a Tafa model 550 hopper, and cooling water was applied and controlled using a PTC model TAE301 heat exchanger unit. Though a two-way powder splitter is very commonly used, finer particles in the powder may experience barrel loading and stick to it before exiting. A three-way powder splitter was therefore used for spraying finer powder to reduce powder pick-up in the barrel. General spray parameters are presented in Table 4.

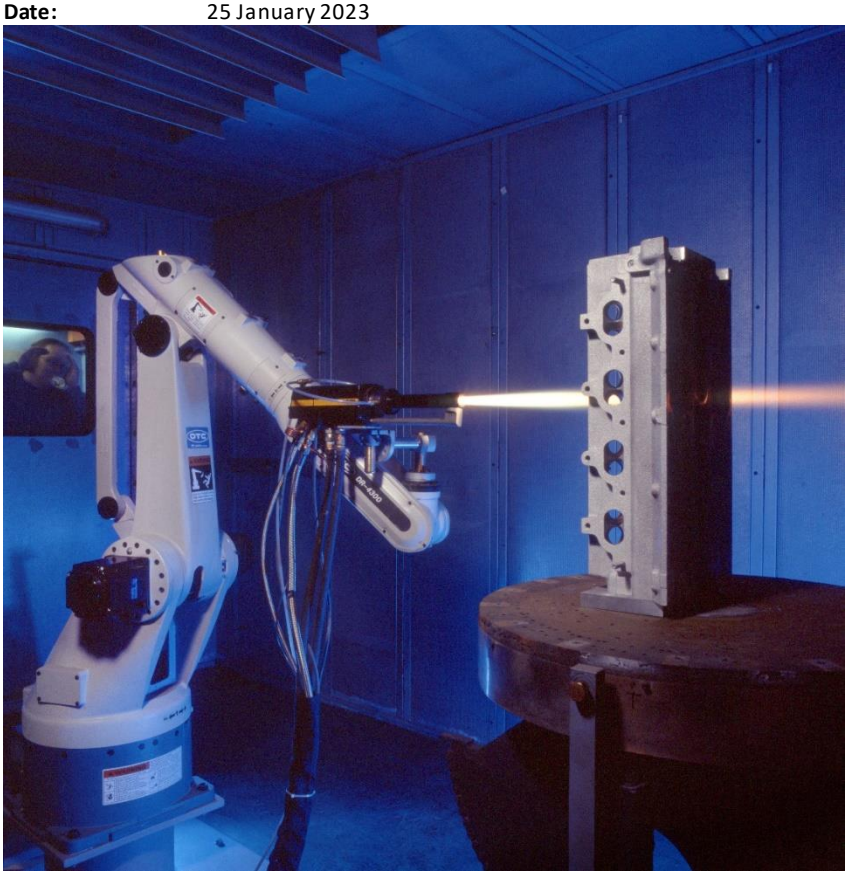

Figure 2 Tafa JP5000 HVOF system (Kerosene) at TWI, Cambridge

Table 4 Fixed spray parameters for JP5000

Spray parameter	Coating systems			
	WC	NiCr-CrC	Self-fluxing	amorphous/nanocrystallian
Powder carrier Gas,	Argon	Argon	Argon	Argon
Powder feed rate, rpm	350	200	150	200
Carrier gas flow rate, scfh	23	28	26	25
Gun tranverse speed, mm/s	900	900	900	900
Increment, mm	5	5	5	5
Nozzle, inch	6	various	4	4
Specimen cooling	air	air	air	air

The development of coatings described in this report reflects work described in the RP1 report and the RP1 review. From Section 1.2, thermal spray is a very complex process. It was deemed not appropriate to attempt to use techniques such as adaptive design of experiments (DoE) and metamodeling to explore various parameter combinations for so many material varieties, which was partly due to high cost and long timescale. A simplified but more effective DoE approach was used to develop suitable parameters for each material type. Key parameters have been covered to identify the preferred spray conditions. All the DoE parameters were set either based on recommended information from suppliers or from TWI's previous experience, including:

- For WC-Co-Cr powder, a standard powder, WOKA 3652, was selected to produce a conventional WC coating for reference. Suitable spray parameters for this powder were identified from TWI's prior experience, as shown in Table 5. For submicron WC-Co-Cr powder, WOKA 3652 FC, round 1 DoE matrix was undertaken at various oxygen and fuel levels to establish suitable combustion environments. Then

round 2 was carried out at a different spray distance and various spray angles to understand how robust the coating is, as the hammer parts to be sprayed are likely to have irregular geometries (Table 6).

- For NiCr-CrC, two powders were selected for the DoE matrix. Powder 1375VF has finer particles than 1375VM which may cause pick-up in the barrel. Therefore in round 1 barrels with different lengths and various oxygen and fuel levels were used to study how they can affect the spraying and coating microstructure. Then more trials were carried out in round 2 using a three-way powder splitter, aiming to reduce blocking issues (Table 7).
- For self-fluxing NiCrFeSiB powder, a similar approach was taken as for powder WOKA 3653FC to selected the best spray condition. Heat treatment of the best coating was also carried out as a feasibility study using an oxy-acetylene torch to check how it affects coating microstructure (Table 8). In this project, self-fluxing coatings will be evaluated in the as-deposited condition and following the fusing (and fluxing) step.
- For amorphous/nanocrystalline powder, SHS 7574HV was selected. A DoE matrix was undertaken at various oxygen and fuel feed rates to establish suitable spraying parameters to achieve a high density and hard coating (Table 9).

Table 5 Standard WC coating using WOKA 3652 powder

Run #	Oxygen flow, SLPM	Kerosene flow, SLPM	Spray distance, mm	Angle, °	Spray sheet
231WC	873	0.4	380	90	20-073

Table 6 DoE conducted for HVOF with WOKA 3652FC POWDER

Run #	Oxygen flow, SLPM	Kerosene flow, SLPM	Spray distance, mm	Angle, °	Spray sheet
232WC1	873	0.400	350	90	20-049
232WC2	920	0.400			20-050
232WC3	920	0.425			20-051
232WC4	920	0.400	380	90	20-081
232WC5			350	70	20-082
232WC6			350	50	20-083
232WC7			350	30	20-084

Table 7 DoE conducted for HVOF with NiCr-CrC 1375VF (4277) and 1375VM (3751) powders

Sample #	Powder	Powder feeder	HVOF	Nozzle.''	Oxygen flow, SLPM	Kerosene flow, SLPM	Spray distance, mm	Spray sheet
233CrC1	4277	2-way	JP5000 ST	4	472	0.23	152	20-025
233CrC2	4277	2-way	JP5000	4	873	0.34	355	20-017
233CrC3	4277	2-way	JP5000	4	873	0.40	355	20-017
233CrC4	3751	2-way	JP5000	6	897	0.32	355	20-040
233CrC5	4277	3-way	JP5000	4	873	0.34	355	20-091
233CrC6	4277	3-way	JP5000	6	873	0.34	355	20-092

Table 8 DoE conducted for HVOF with NiCrFeSiB 1660-02 powder

Sample #	Oxygen flow, SLPM	Kerosene flow, SLPM	Spray distance, mm	Spray angle, °	Time, min	Spray sheet
234Flux1	897	0.385	380	90	-	20-052
234Flux2	930	0.350	380	90	-	20-053
234Flux3	930	0.385	380	90	-	20-054
234Flux4	897	0.350	380	90	-	20-055
234Flux5	930	0.385	350	90	-	20-084
234Flux6			380	70	-	20-085
234Flux7			380	50	-	20-087
234Flux8			380	30	-	20-088
234Flux9S	930	0.385	380	90	3	20-186

234Flux9L			380	90	5	20-186

Table 9 DoE conducted for HVOF with amorphous/nanocrystalline SHS 7574HV powder

Sample #	Oxygen flow, SLPM	Kerosene flow, SLPM	Spray distance, mm	Spray angle, °	Spray sheet
235Amor1	920	0.400	356	90	20-066
235Amor2	920	0.370	356	90	20-067
235Amor3	920	0.330	356	90	20-068
235Amor4	873	0.370	356	90	20-069
235Amor5	873	0.330	356	90	20-070
235Amor6	897	0.370	356	90	20-071

2.3 Characterisation

2.3.1 Overview

The performance of the deposited samples was assessed in terms of coating characteristics and mechanical performance using a combination of the following tests to select the best process parameters.

2.3.2 Surface roughness

Samples were measured using an Alicona InfiniteFocus SL 3D surface profilometer. The surface information was gathered by moving the optics relative to the sample while continuously imaging the surface. Height information was then determined from the regions of the images which are in focus. The measurement was done based on BS EN ISO 4288. At least three measurements were done for each sample and an average value was taken.

2.3.3 Deposition efficiency

Deposition efficiency (D.E.) was measured mainly by weight deposited per minute. It was calculated from the weight changes of samples before and after being sprayed. At least three specimens were used for each sample.

For a few coatings, it was evaluated as thickness deposited per pass. Coating thickness was determined from measurements made on cross-sections of each coating. The coating thickness was then divided by the total number of passes. At least ten thickness measurements were taken for each sample.

2.3.4 Coating porosity

Coating porosity was measured according to ASTM E2109-01:2007 Standard. The cross-sectioned samples were cold-mounted in epoxy, ground with silicon carbide papers with various grits then polished with diamond (3 and 1 µm) and colloidal silica (0.02 µm) suspensions. Optical microscopy was used to take microstructure images on the polished cross-section surfaces. Porosity was calculated by area fraction analysis and thresholding of at least twenty micrographs using ImageJ software. An average value was taken.

2.3.5 Microstructure characterisation

For powder and coating microstructural analysis, scanning electron microscopy (SEM) equipped with energy dispersive X-ray spectroscopy (EDX) was used. Images at different magnifications were taken, mainly in backscattered mode for higher contrast between pores, oxide areas and metal matrix. EDX spectroscopy was employed while imaging on SEM to obtain the elemental compositions at different areas of the sample cross-sections.

2.3.6 Hardness

Micro-hardness was taken on the prepared coating cross-section surfaces using a Duramin Vickers hardness tester, manufactured by Struers in accordance with BS EN ISO 6507-1:2005. A load of 300g was used and at least ten indents were made along the coating length. The hardness value was expressed as an average value with a standard deviation.

2.3.7 Adhesion strength

Adhesion strength of deposited coatings was measured using pull-off adhesion testing according to ASTM C633. The test determines the adhesion strength of a coating to a substrate, or the cohesive strength of the coating, in tension normal to the surface. The coated samples were bonded onto dollies with a testing area of 25.4mm diameter. The load was applied using an Instron machine, up to the point at which bonding failure occurred. The joint was then examined to determine the location of failure and classified as occurring at either the coating to the substrate interface, within the coating or within the epoxy adhesive. Five samples were tested for each coating and the failure stress was expressed as a mean of five results with a standard deviation.

3. RESULTS

3.1 WC-based coatings

3.1.1 Powders

The microstructures of the WC powders and their bulk EDX analyses are shown in Figure 3 (WOKA 3652) and Figure 4 (WOKA 3652FC). It can be seen that both powders have a spherical and porous morphology, which is favourable for achieving good flow during spraying. A small proportion of irregular particles can be found for WOKA 3652FC (nominal size: -45+15µm). Both powders use Co and Cr as binders that are homogeneously distributed among various grains.

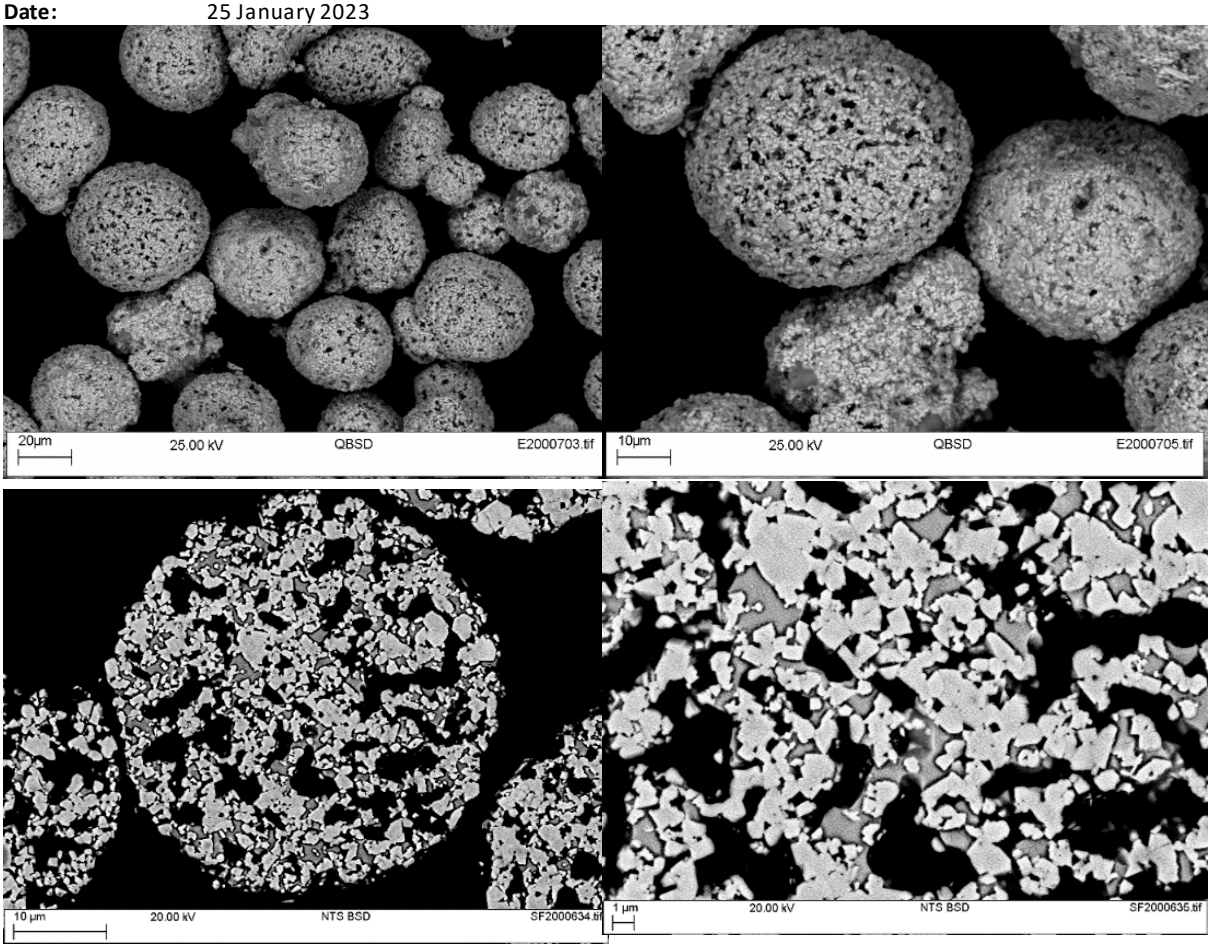

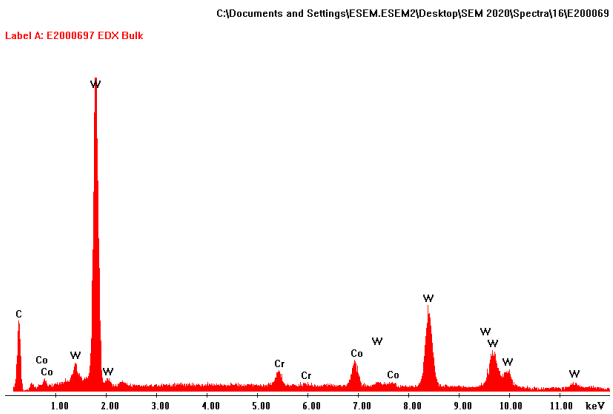

Figure 3 SEM and EDX analyses of as-received powder 4091, Woka 3652

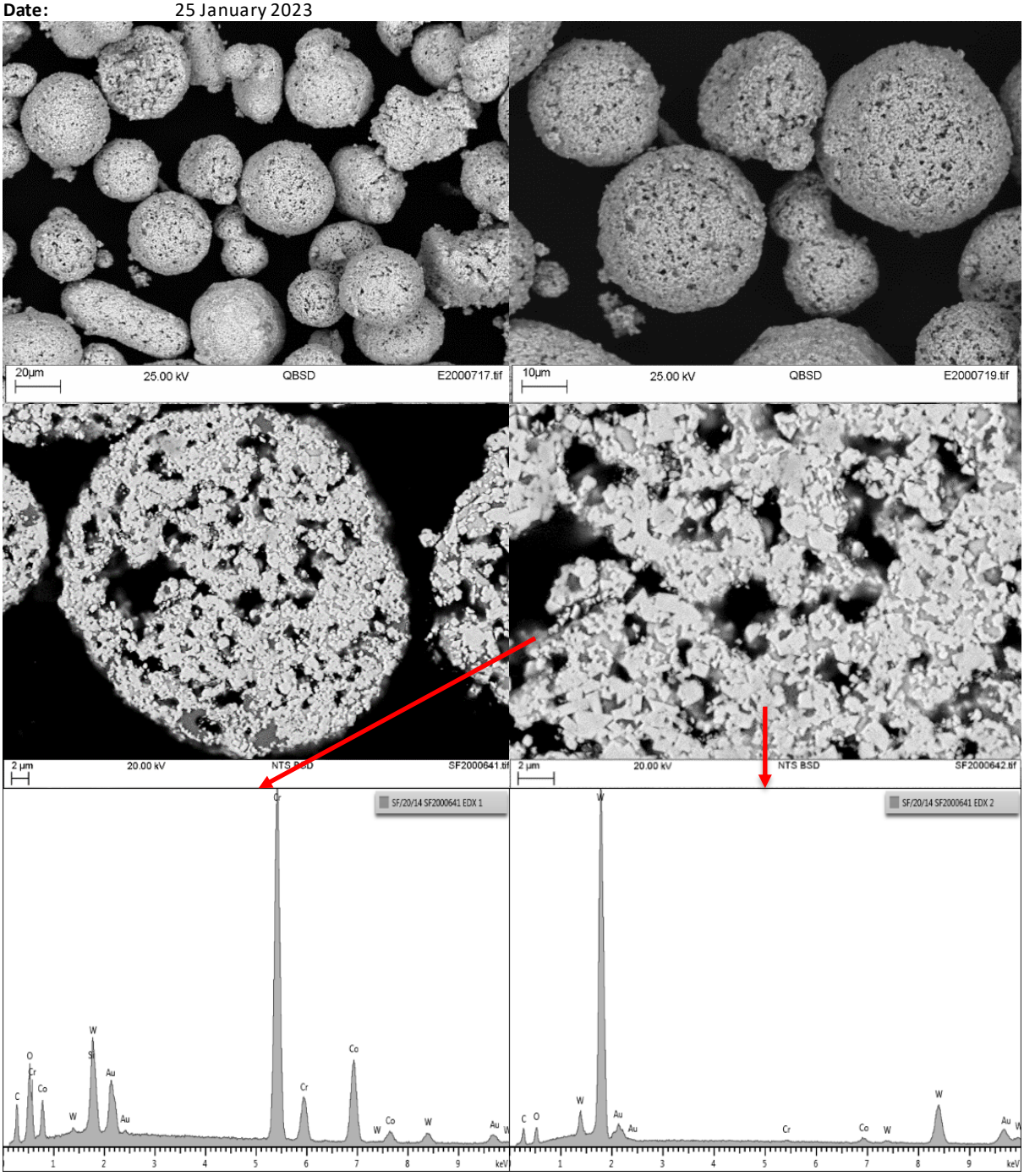

Figure 4 SEM and EDX analyses of as-received powder 4278, Woka 3652FC

3.1.2 Coatings

3.1.2.1 Standard WC coating

Microstructure of WC coating (231WC) deposited from standard WC powde, WOKA 3652, is shown in Figure 5, indicating a fairly uniform coating. However, a few cracks can be seen on the coating top surface, which might be caused during metallographic preparation due to the brittleness of the coating. Coating 231WC has average surface roughness Ra around 4.0 µm, with porosity of 5.4 ± 0.7% and hardness of 1252±124 $HV_{0.3}$ (Table 10).

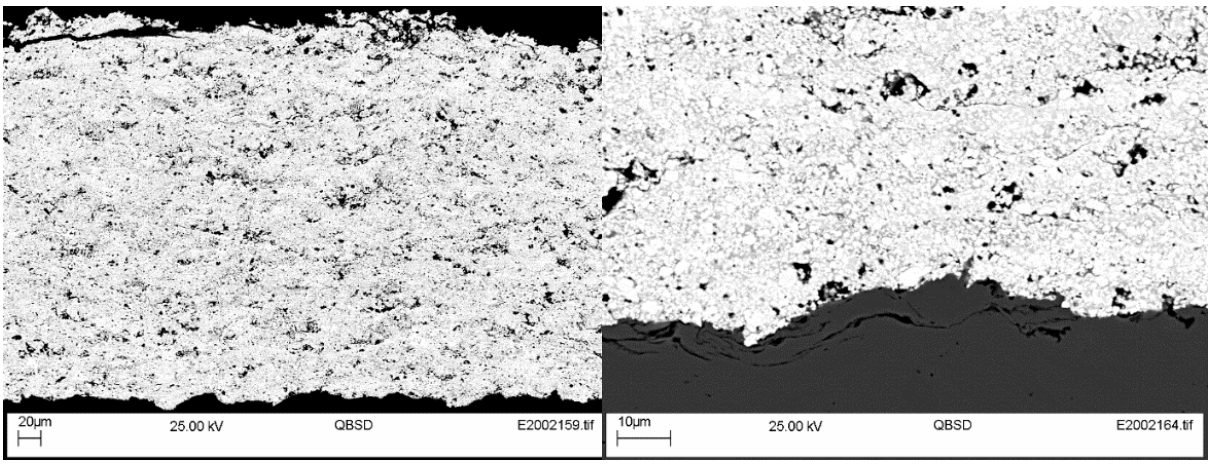

Figure 5 SEM micrographs of Coating 231WC in back-scatter mode

Table 10 Test results of standard WC coating with 4091 powder

Run #	Oxygen flow, SLPM	Kerosene flow, SLPM	Ra, µm		Rz, µm		Porosity, %		Hardness, HV0.3	
			Ave	Dev	Ave	Dev	Ave	Dev	Ave	Dev
231WC	873	0.400	4.0	0.4	25.7	2.1	5.4	0.7	1252	124

3.1.2.2 Coating development

The cross-sectional micrographs reveal that coatings deposited from WC powder WOKA 3652FC have finer microstructure than coating 231WC deposited from standard WC powder, WOKA 3652 (Figure 6-Figure 12).

When sprayed under different oxygen and kerosene flow rates, the coatings do not seem to show big differences regarding their surface roughness, which are similar to standard coating 231WC (Table 11). All coatings show good contact along the steel substrate profile and with high deposit efficiency from 47 to 51% (Figure 6-Figure 9, Table 12). Those coatings have different levels of porosity ranging from 0.9±0.3 to 4.4±1.0%, which is normally formed due to insufficient particle deformation at the impact and/or insufficient particle velocity. Porosity level for thermal sprayed coatings is very important for their corrosion performance and the lowest porosity is always preferred. Therefore, the best parameters of those tested for WC powder WOKA 3652 are coating 232WC2 that had the lowest porosity of 0.9% and highest hardness of 1218±112$HV_{0.3}$.

To check how robust WC coating is when parts with complex geometries need to be sprayed, different spray distances and spray angles were studied. Spraying under different spray angles from 90° to 30°, coating surface roughness Ra decreases from 4.3 µm to 3.0 µm and Rz decreases from 27.2 µm to 17.7 µm. Reducing spray angles from 90° to 50° does not seem to have a significant effect on coating deposition efficiency, but a big drop from 45 to 38% was seen when the spray angle decreased from 50° to 30°(Table 12). Coating porosity seems to be very sensitive with parameter changes, all increased than coating 232WC2 when being sprayed at 90°. Hardness of WC coating is relatively comparable when deposition angle is reduced from 90° to 70°. Spray distance seems to be very sensitive for WC powder. When spray distance was increased from 350 to 380mm, coating porosity increased from 0.9±0.3 to 7.8±0.6% and hardness dropped from 1218±112 to 1103±210HV_{03}. Therefore, spraying condition seems to be very sensitive for WC powder and parameters should be very carefully chosen when irregular shaped parts need to be sprayed at later stage of the project.

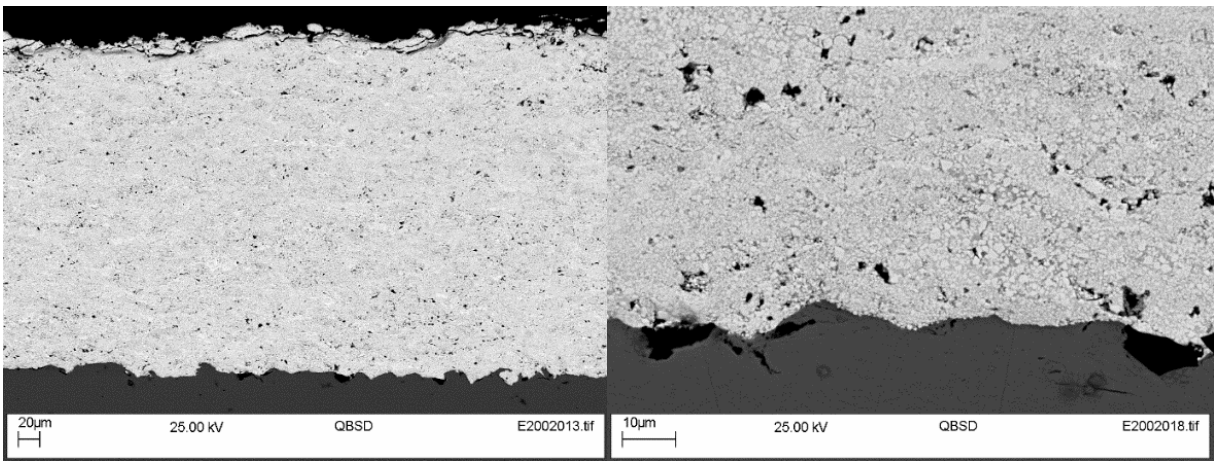

Figure 6 SEM micrographs of Coating 232WC1 in back-scatter mode

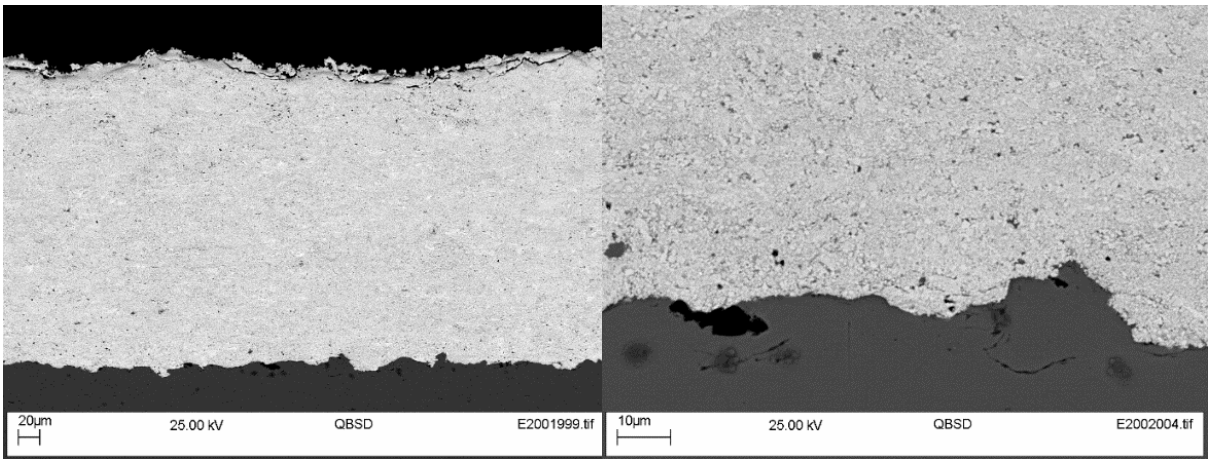

Figure 7 SEM micrographs of Coating 232WC2 in back-scatter mode

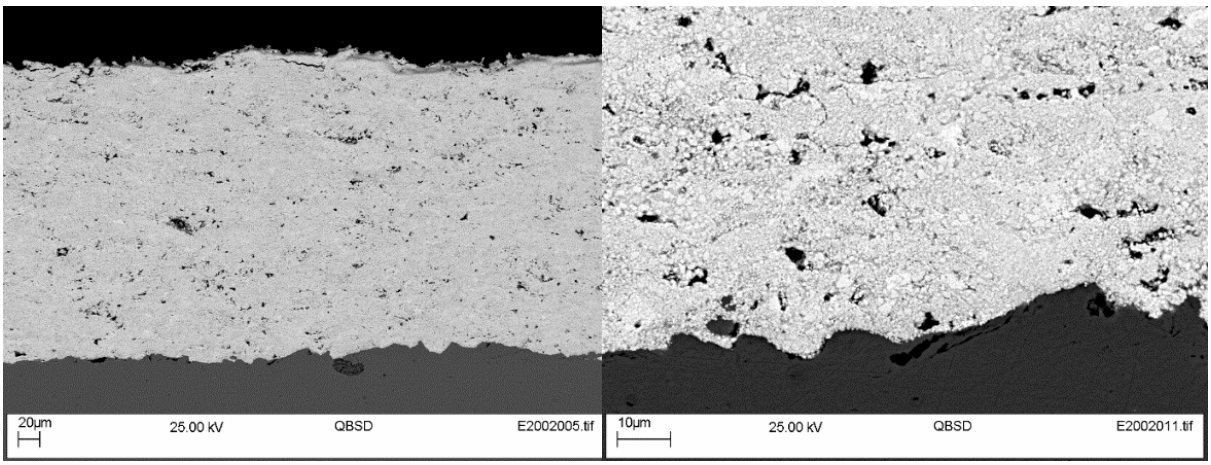

Figure 8 SEM micrographs of Coating 232WC3 in back-scatter mode

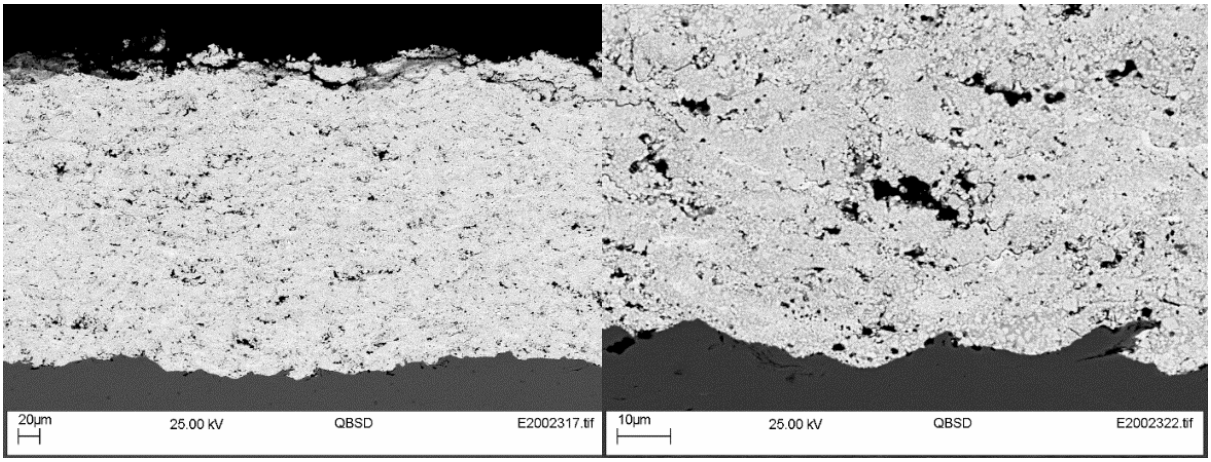

Figure 9 SEM micrographs of Coating 232WC4 in back-scatter mode

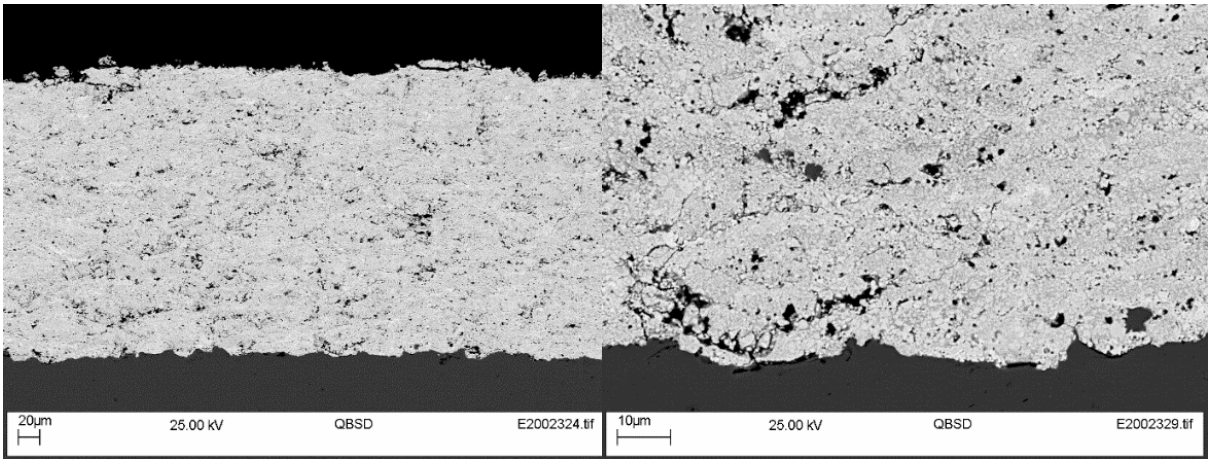

Figure 10 SEM micrographs of Coating 232WC5 in back-scatter mode

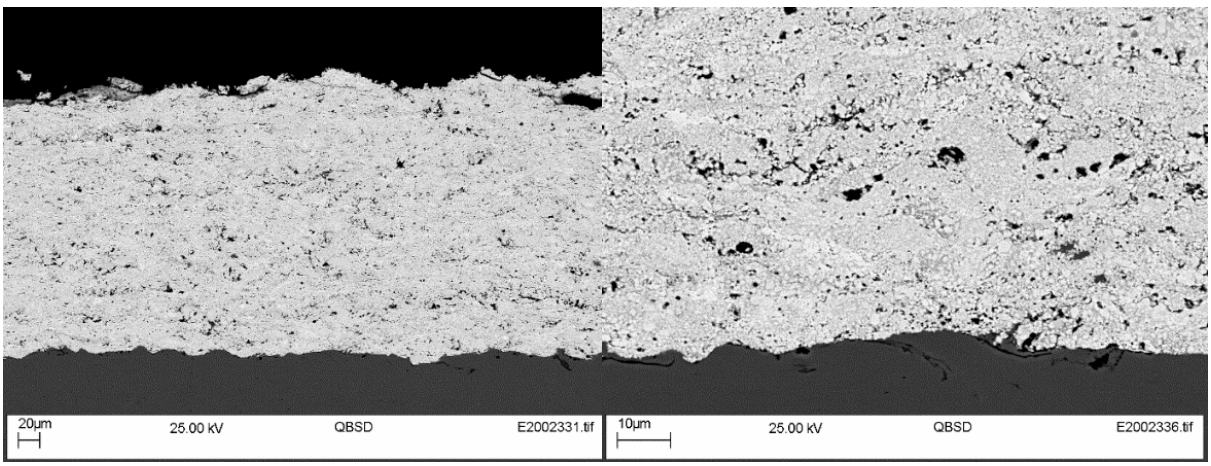

Figure 11 SEM micrographs of Coating 232WC6 in back-scatter mode

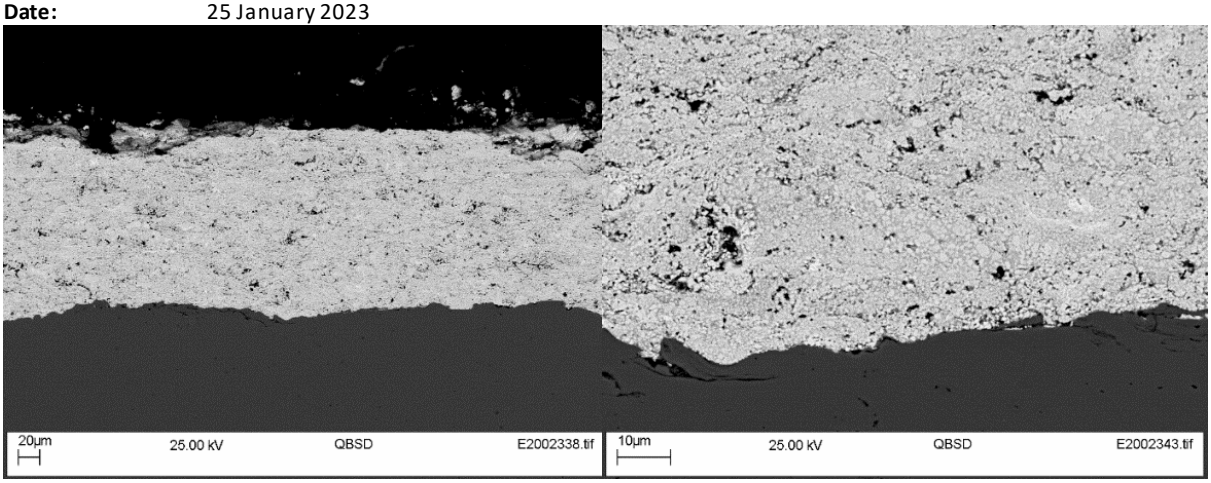

Figure 12 SEM micrographs of Coating 232WC7 in back-scatter mode

Table 11 As-deposited coating surface roughness of DoE matrix with 4278 powder

Run #	Oxygen flow, SLPM	Kerosene flow, SLPM	Spray distance, mm	Angle, °	Ra, µm		Rz, µm	
					Ave	Dev	Ave	Dev
232WC1	873	0.400	350	90	3.8	0.2	23.2	2.2
232WC2	920	0.400			4.3	0.5	27.2	3.6
232WC3	920	0.425			4.2	0.5	25.5	2.7
232WC4	920	0.400	380	90	4.2	0.3	24.3	1.5
232WC5			350	70	3.7	0.2	22.3	1.8
232WC6			350	50	3.6	0.5	21.7	1.9
232WC7			350	30	3.0	0.0	17.7	0.6

Table 12 Test results of DoE matrix with 4278 powder

Run #	Oxygen flow, SLPM	Kerosene flow, SLPM	Spray distance, mm	Angle, °	D.E., %	Porosity, %		Hardness, $HV_{0.3}$	
						Ave	Dev	Ave	Dev
232WC1	873	0.400	350	90	53	2.4	0.7	1095	132
232WC2	920	0.400			51	0.9	0.3	1218	112
232WC3	920	0.425			47	4.4	1.0	1159	176
232WC4	920	0.400	380	90	49	7.8	0.6	1103	210
232WC5			350	70	49	6.0	0.6	1195	108
232WC6			350	50	45	6.1	0.5	1139	119
232WC7			350	30	38	5.1	0.8	971	194

3.2 NiCr-CrC based coatings

3.2.1 Powders

SEM images of CrC-NiCr powder 1375VM and 1375VF are shown in Figure 13 and Figure 14, respectively. It can be seen that powder 1375VM with norminal size range of 15 to 45 µm has irregular shape, while powder 1375VF with norminal size range of -45+11 µm presents mostly a spherical agglomerated shape with a lot of fine particles. Both powders are composed of porous particles. Cross-sectioned SEM images and EDX analysis show that both powders have homogeneously mixed two phases, with the presence of different contrast zones under back-scattered mode. The dark contrast features are found to be Cr and C rich by EDX analysis, while the bright contrast matrix phase is rich in Ni and Cr, which functions as the binder phase.

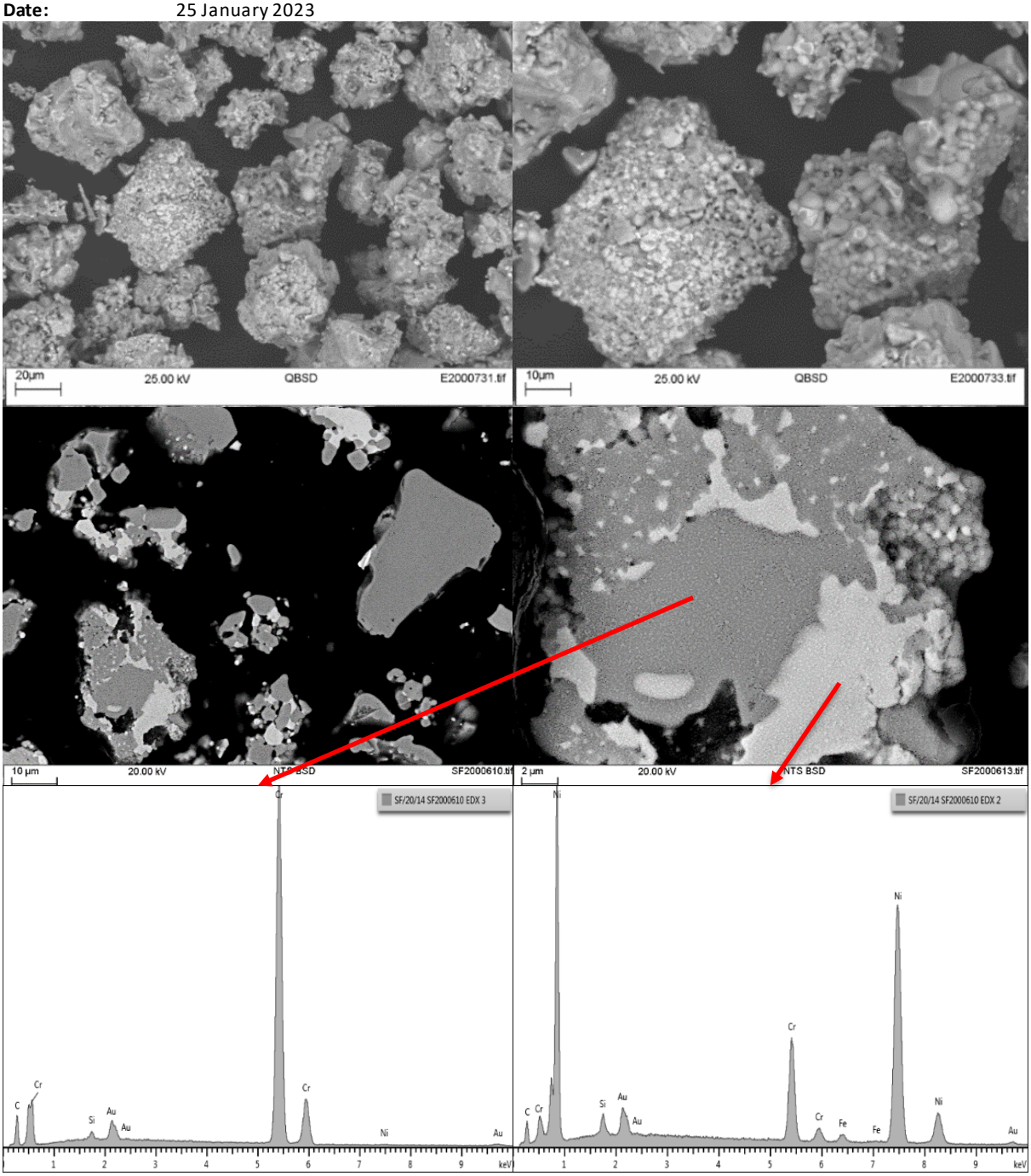

Figure 13 SEM and EDX analyses of as-received powder 3751, 1375VM

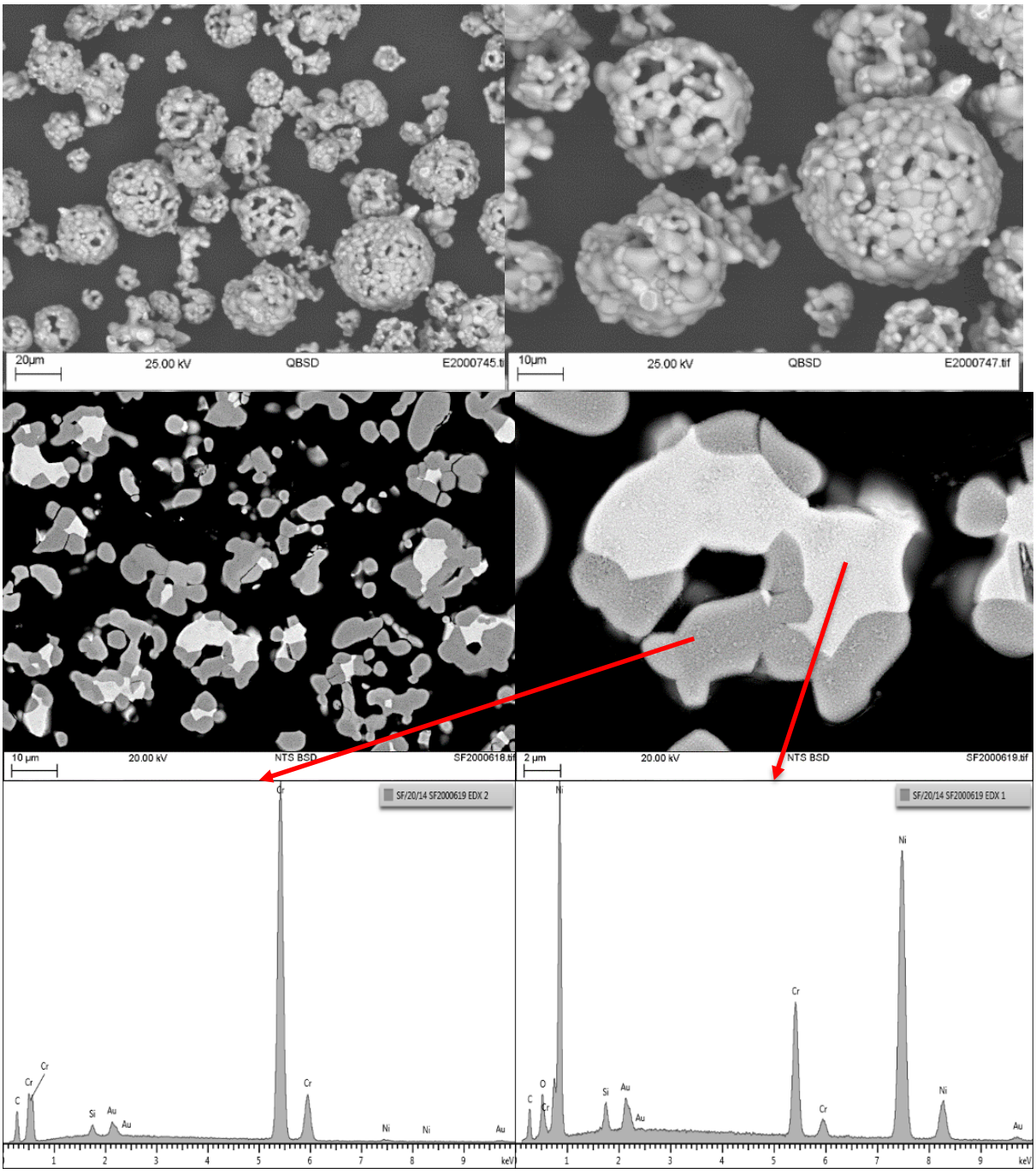

Figure 14 SEM and EDX analyses of as-received powder 4277, 1375VF

3.2.2 Coatings

From SEM and EDX analysis (Figure 15 - Figure 20), all CrC-NiCr coatings generally show a laminar microstructure with the presence of a small level of voids of approximately micron size. They comprise a metallic binder Ni-Cr region (bright areas) with carbide CrC phase (dark areas). All coatings seem to have a continuous contact along the substrate profile, indicating good adhesion between coating and substrate. However, their characteristics seem to vary significantly when deposited under different parameters.

Though powder 1375VF is designed for the JP5000 – ST system, it can also be used with the Standard JP5000 gun, which has potential to offer a much smoother and denser coating. The powder was firstly tried with the JP5000 – ST gun and the resulting coating, 233CrC1, has a very dense structure, and the highest hardness and deposit efficiency compared with others (Table 14, Figure 15). There is no evidence of cracking in this coating. However, its surface roughness is about 5 times higher than those sprayed with the JP5000 system (Table 13). Surface roughness plays an important role in the lifespan of coated components. Higher surface roughness normally leads to higher material loss, which is not favourable to its wear and erosion-corrosion resistance [8]. Coatings 233CrC2 and 233CrC3 were then sprayed using standard JP5000 gun, with different fuel flow rates. Both coatings present much lower surface roughness than 233CrC1 (3.7±0.1 and 3.2±0.1 vs 17.5±1.5μm) (Table 13). However, cracking in the coating or discontinuity of splats on the coating surface are found for both coatings, indicating lack of cohesive strength (Figure 16, Figure 17). This might be caused by lower flame temperature or insufficient velocity of the flame. However, blocking in the nozzle was seen during the positioning process due to the high level of fine particles in this powder. This indicates that higher combustion pressure or temperature would not be favourable for maintaining good flow of this powder.

Powder 1375VM is a more commonly used powder for the JP5000 system as designed by Praxair. The deposited coating 233CrC4 presented very uniform structure without obvious cracks on the surface, but it also has too high a surface roughness Ra of about 10.3 μm (Figure 18, Table 13). Furthermore, its deposit efficiency is much lower and its hardness is only about two thirds of those coatings deposited from 1375VF (Table 14).

In order to reduce blocking of the nozzle and also achieve a good quality coating, a three-way powder splitter was used for coating 233CrC5, 233CrC6 and 233CrC7. Coating 233CrC5 was deposited under the same parameters as 233CrC2, which resulted in a slightly denser coating, with fewer loosely cohered splats on the surface (Figure 19). When the longer 6 inch nozzle was used, the coating (233CrC6) became more compact and no obvious cracking or discontinuity of splats on the surface were observed, indicating improved cohesive strength (Figure 20). Meanwhile, compared with 233CrC5, its deposit efficiency is slightly improved from 35% to 38%, porosity decreases from 1.5% to 1.1%, hardness increases from 722±58 to 755±72$HV_{0.3}$, and adhesion strength increases from 65.0±8.3 to 73.9±10.3 MPa (Figure 20, Table 14, Table 15). No blocking was observed during spraying for either condition when a three-way powder splitter was used. Therefore, coating 233CrC6 was selected as the best CrC-NiCr coating, of the process conditions used, for its overall performance.

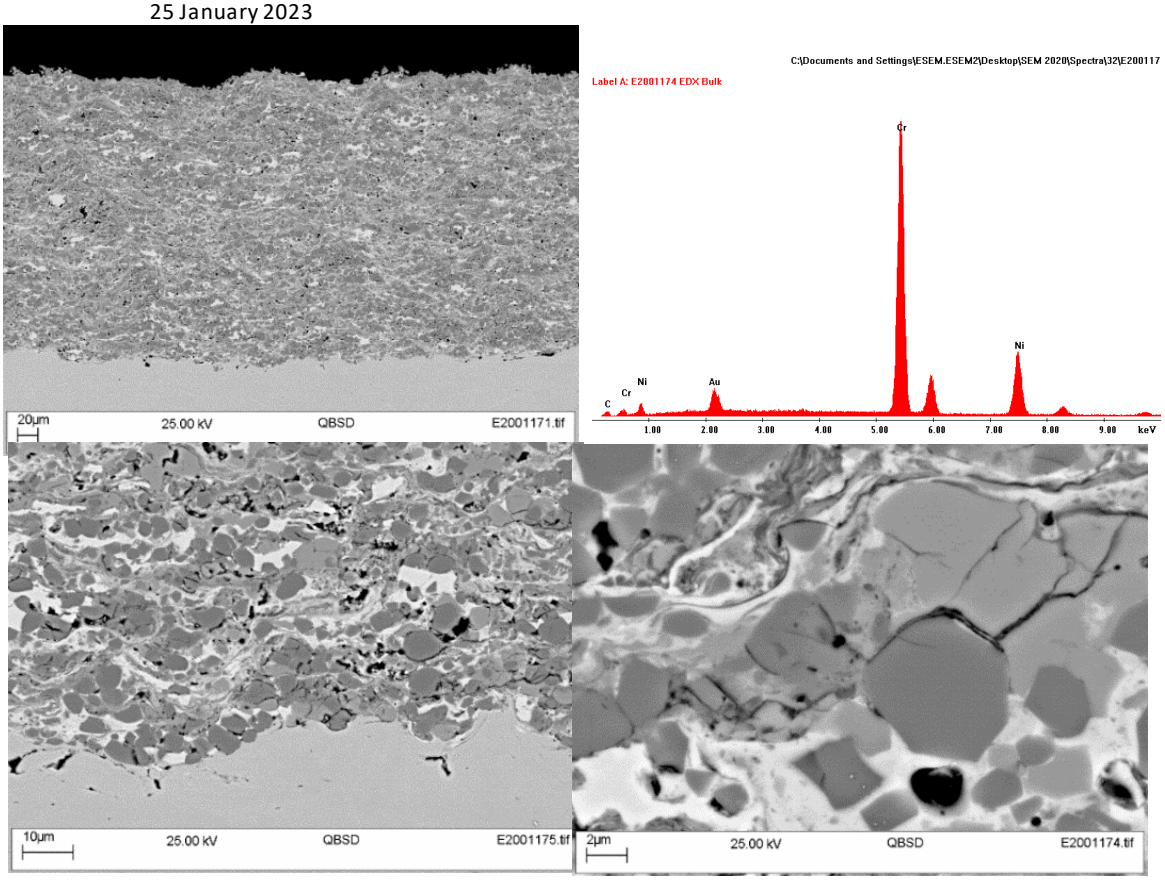

Figure 15 SEM micrographs of Coating 233CrC1, with EDX spectrum

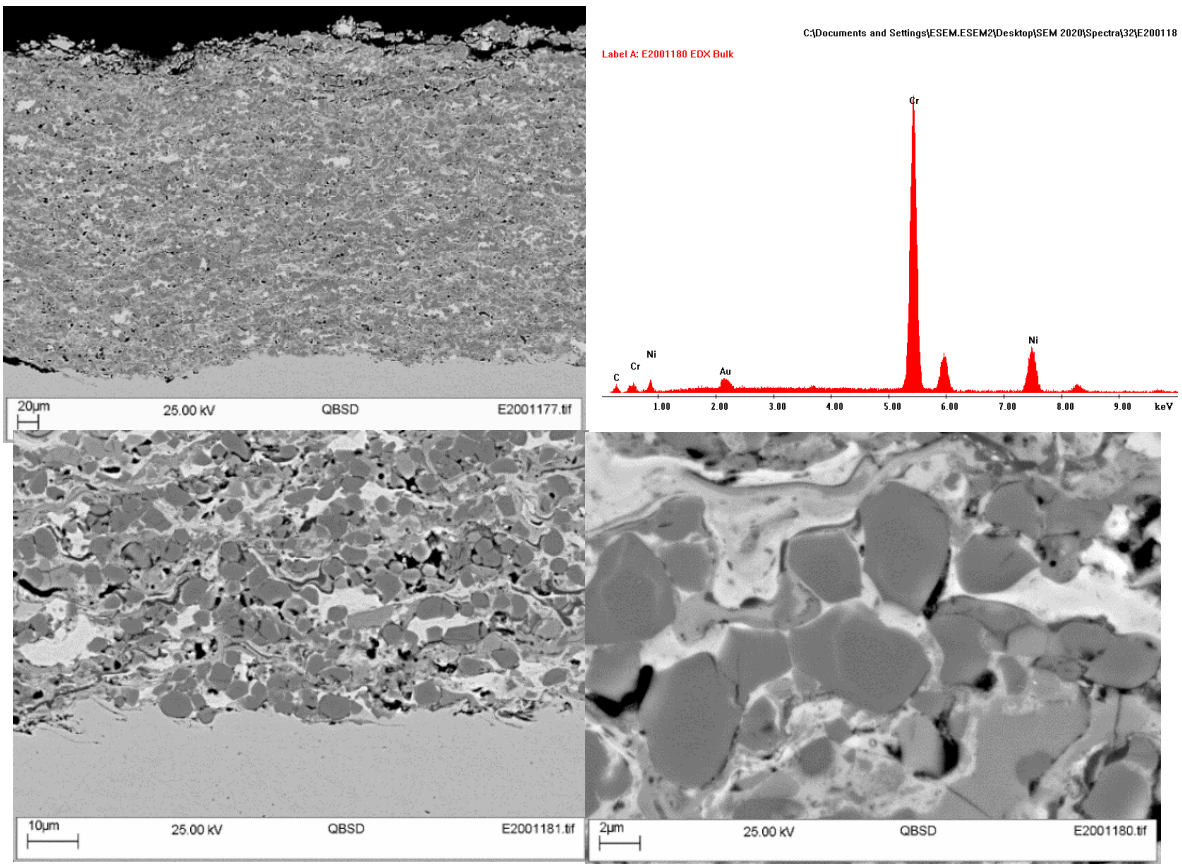

Figure 16 SEM micrographs of Coating 233CrC2, with EDX spectrum

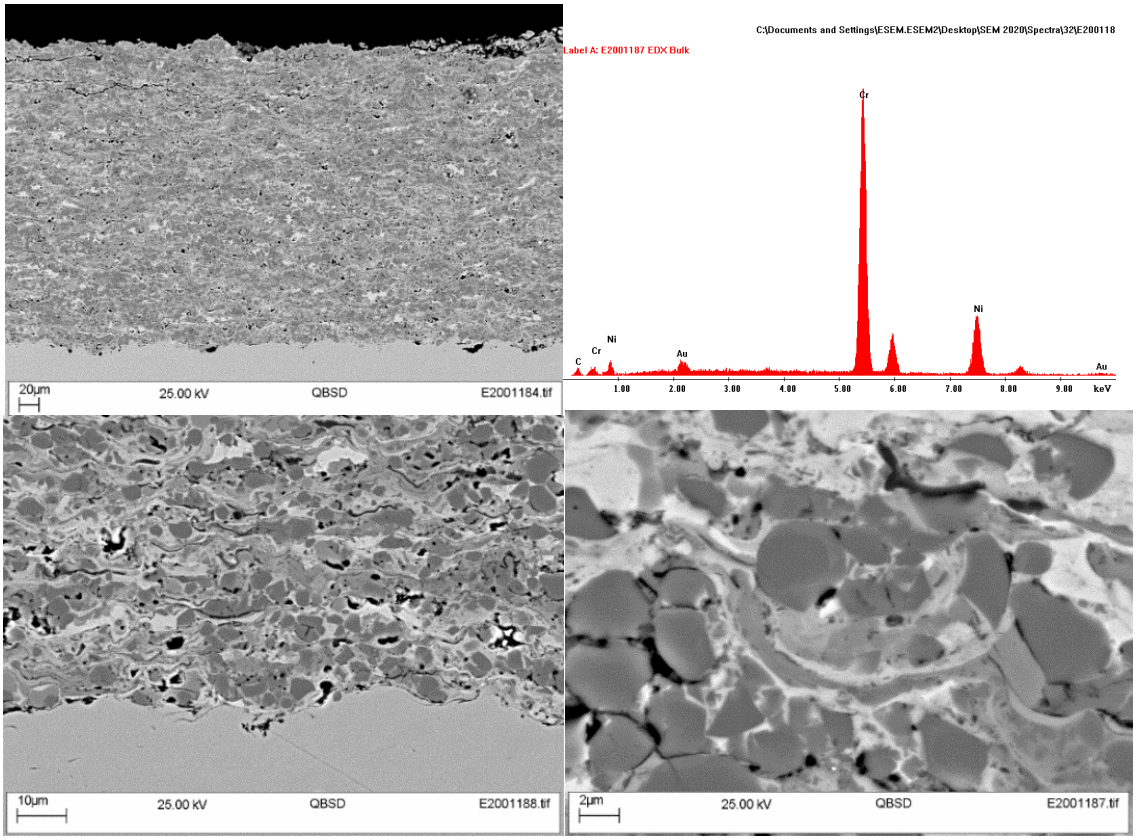

Figure 17 SEM micrographs of Coating 233CrC3.0, with EDX spectrum

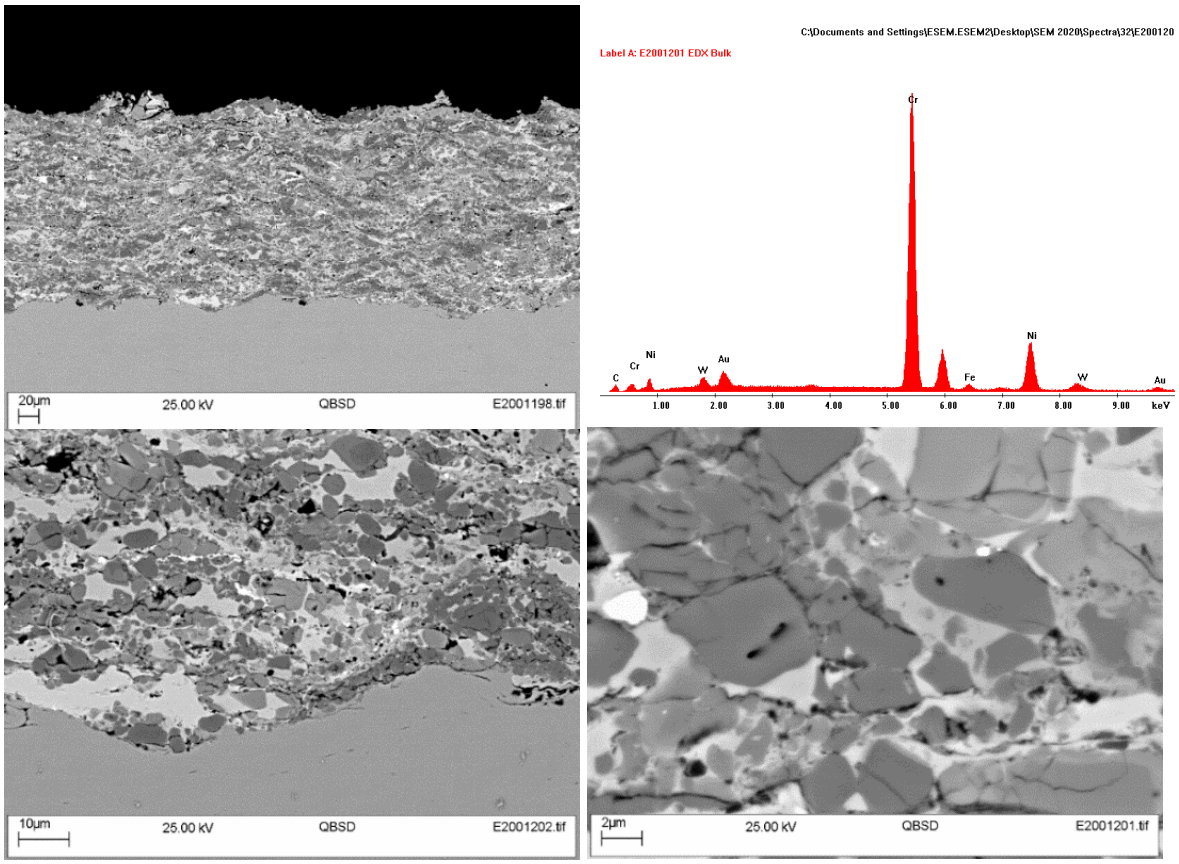

Figure 18 SEM micrographs of Coating 233CrC4, with EDX spectrum

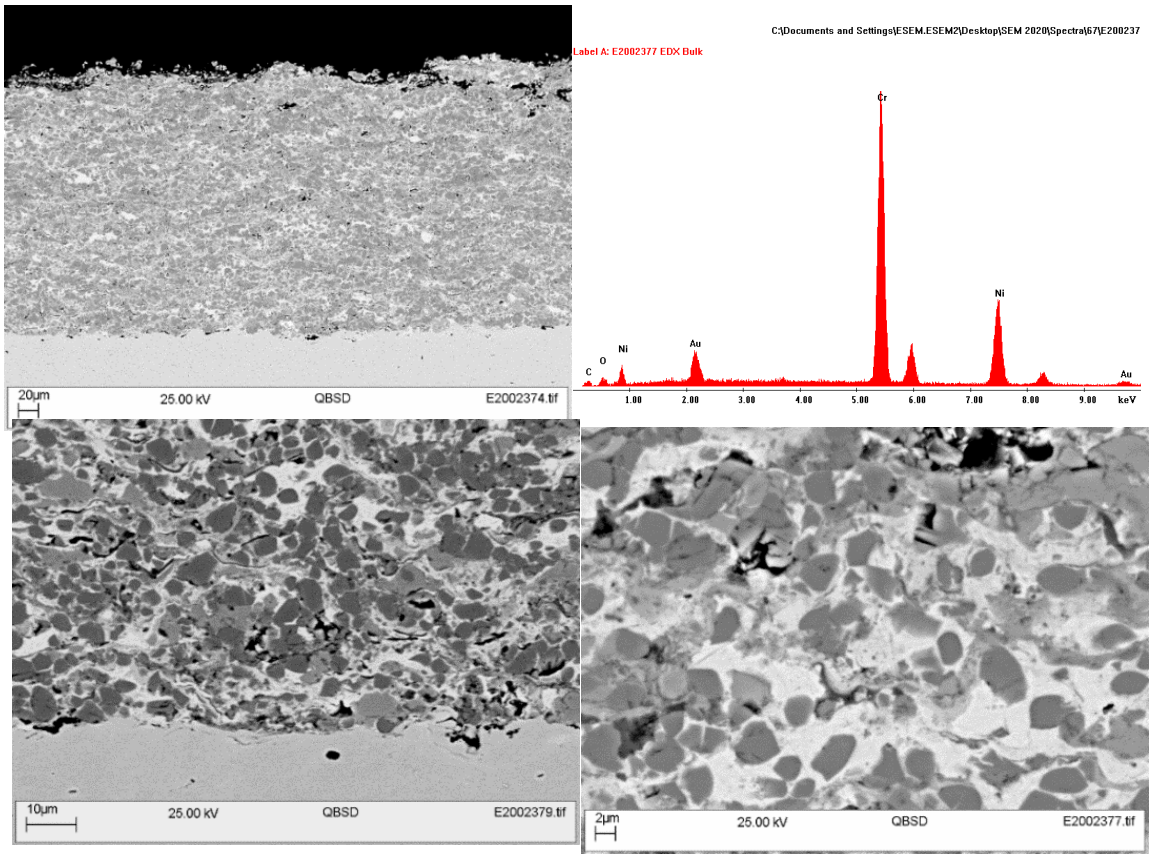

Figure 19 SEM micrographs of Coating 233CrC5, with EDX spectrum

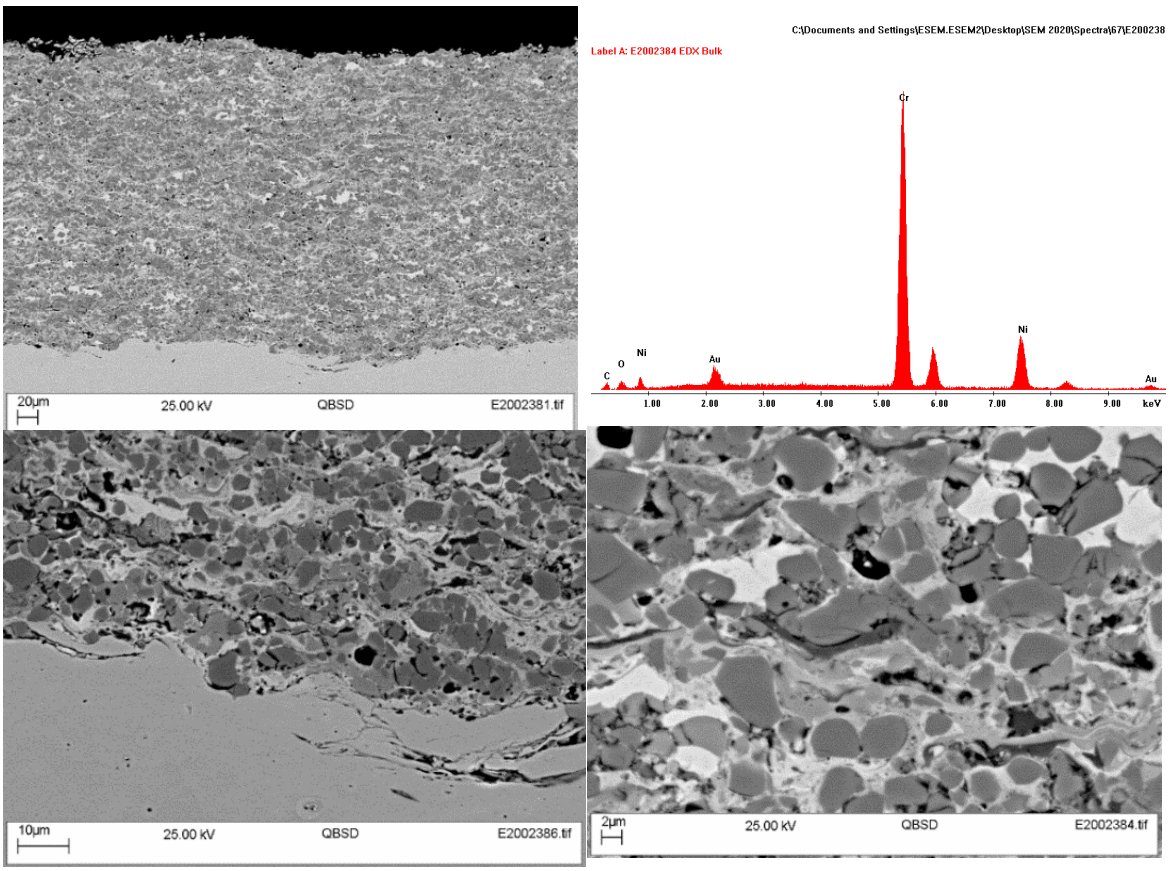

Figure 20 SEM micrographs of Coating 233CrC6, with EDX spectrum

Table 13 As-deposited coating surface roughness of DoE matrix with $75Cr_3C_2$/25NiCr powders

Sample # Round 1	Powder	Powder feeder	Nozzle, inch	Oxygen flow, SLPM	Kerosene flow, SLPM	Ra, µm		Rz, µm	
						Ave	Dev	Ave	Dev
233CrC1	4277	2-way	4	472	0.23	17.5	1.5	104.7	9.2
233CrC2	4277	2-way	4	873	0.34	3.7	0.1	22.3	0.2
233CrC3	4277	2-way	4	873	0.40	3.2	0.1	19.7	0.6
233CrC4	3751	2-way	6	897	0.32	10.3	0.8	69.6	7.8
233CrC5	4277	3-way	4	873	0.34	3.8	0.1	22.9	2.2
233CrC6	4277	3-way	6	873	0.34	3.5	0.7	21.5	2.6

Table 14 Test results of DoE matrix with $75Cr_3C_2$/25NiCr powders

Sample #	Powder	Powder feeder	Nozzle, inch	Oxygen flow, SLPM	Kerosene flow, SLPM	Thickness per pass, µm	D.E., %	Porosity, %		Hardness, HV0.3	
								Ave	Dev	Ave	Dev
233CrC1	4277	2-way	4	472	0.23	9.1	-	1.0	0.3	975	62
233CrC2	4277	2-way	4	873	0.34	6.3	-	1.7	0.3	846	59
233CrC3	4277	2-way	4	873	0.40	6.1	-	1.6	0.1	927	63
233CrC4	3751	2-way	6	897	0.32	2.4	-	1.8	1.2	587	140
233CrC5	4277	3-way	4	873	0.34	5.2	35	1.5	0.2	722	58
233CrC6	4277	3-way	6	873	0.34	6.0	38	1.1	0.1	755	72

Table 15 Adhesion strength of $75Cr_3C_2$/25NiCr coatings

Sample #	Powder	Powder feeder	Nozzle. inch	Oxygen flow, SLPM	Kerosene flow, SLPM	Adhesion strength, MPa	
						Ave	Dev
233CrC1	4277	2-way	4	472	0.23	-	-
233CrC2	4277	2-way	4	873	0.34	70.4	6.0
233CrC3	4277	2-way	4	873	0.40	-	-
233CrC4	3751	2-way	6	897	0.32	-	-
233CrC5	4277	3-way	4	873	0.34	65.0	8.3
233CrC6	4277	3-way	6	873	0.34	73.9	10.3

3.3 Self-fluxing coatings

3.3.1 Powder

SEM and EDX analysis of self-fluxing powder 1660-02 show that this gas-atomised powder has primarily spherical particle shape (Figure 21). The powder has homogeneously mixed two phases, with dark contrast Cr rich features and bright contrast Ni-rich matrix.

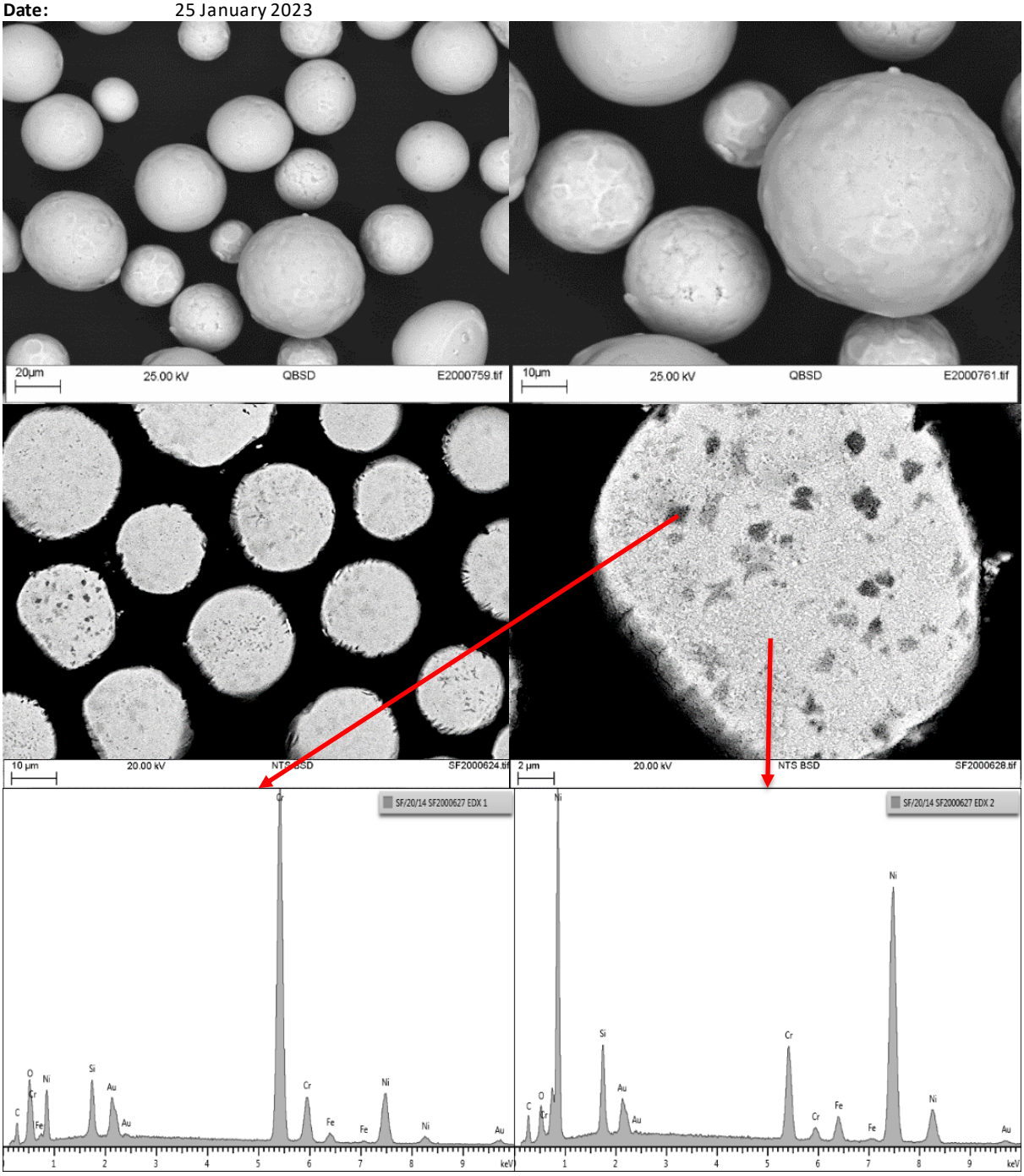

Figure 21 SEM and EDX analyses of as-received powder 4279, 1660-20

3.3.2 Coatings

From coating microstructure analysis, it seems that different fuel and oxygen flow rates do not have a significant effect on the coating microstructure (Figure 22-Figure 25). All four coatings presented some horizontal microcracks through the coating thickness. The appearance of those cracks can possibly be explained by the differences in the values of coefficients of thermal expansion between different phases. The surface roughness of deposited self-fluxing coatings under different fuel and oxygen flow rates are very similar, with Ra varying between 5.8 and 6.9µm and Rz in the range of 37.2 to 41.7 µm (Table 16). Adhesion strength of the coatings was also being tested under standard ASTM C633, where coating 234Flux4 has the highest adhesion strength and coating 234Flux3 has the second highest (Table 17). Their deposition efficiency is very similar, ranging from 53 to 59%. Coating 234Flux3 presents the lowest porosity of 2.4% among four coatings. Different fuel and

oxygen flow rates do not have much effect on the coating's hardness, which ranges from 657±108 to 684±56 $HV_{0.3}$, in a similar range to those reported in literature [9]. Therefore, coating 234Flux3 seems to be the best of those evaluated for its overall performance with lowest porosity, good adhesion strength and hardness.

In order to study the robustness of self-fluxing alloy when a complex shaped parts needs to be sprayed, coating performance under a different spray distance and different spray angles was also checked. Decreasing spray distance does not have much influence on surface roughness but produces a denser and harder coating (Figure 26, Table 16, Table 18). When spray angle drops from 90° to 30°, coating surface roughness Ra only slightly decreases from 6.4±0.4 to 5.9±0.3% (Table 16). However, their deposition efficiency decreases dramatically from 56% to 35%. While coating porosity does not change significantly, the coating sprayed at 30° is delaminated from the substrate as can be seen from its SEM images (Figure 26-Figure 29, Table 18). Though hardness seems to be good for all these coatings, adhesion strength is also very critical to their performance. Therefore, self-fluxing coating should not be sprayed at a spray angle of around 30° during later stages of the project.

Post heat treatment was also carried out to study how this would affect the coating microstructure; this decreases the porosity and promotes sintering of self-fluxing alloys. The liquid phase appears between 900-1000°C for Ni-based self-fluxing alloy [10]. Both coatings with different heat treatment times show that their surface becomes smoother and their microstructure become much denser (Figure 30, Figure 31, Table 16). From their microstructure images, some needle/irregular shaped phases were formed after heat treatment. This can be caused by the reaction of boron and silicon in the alloy with oxides at high temperatures, which forms low melting point borosilicate that prevents further oxidation of active elements in the alloys and enhances wear resistance of such coating [6]. Correspondingly, hardness of the fused coatings is increased from 661±68 to 863±53$HV_{0.3}$. Adhesion strength of fused coatings was not tested in this study but it has been reported to be 10 times higher than their as-sprayed conditions due to the metallurgical bonding compared with pure mechanical bonding [11]. This is only a feasibility study to check how heat treatment can affect the microstructure of self-fluxing alloy; heat treatment will not be applied to the hammer prototype if the as-sprayed condition performs well in WP3's testing.

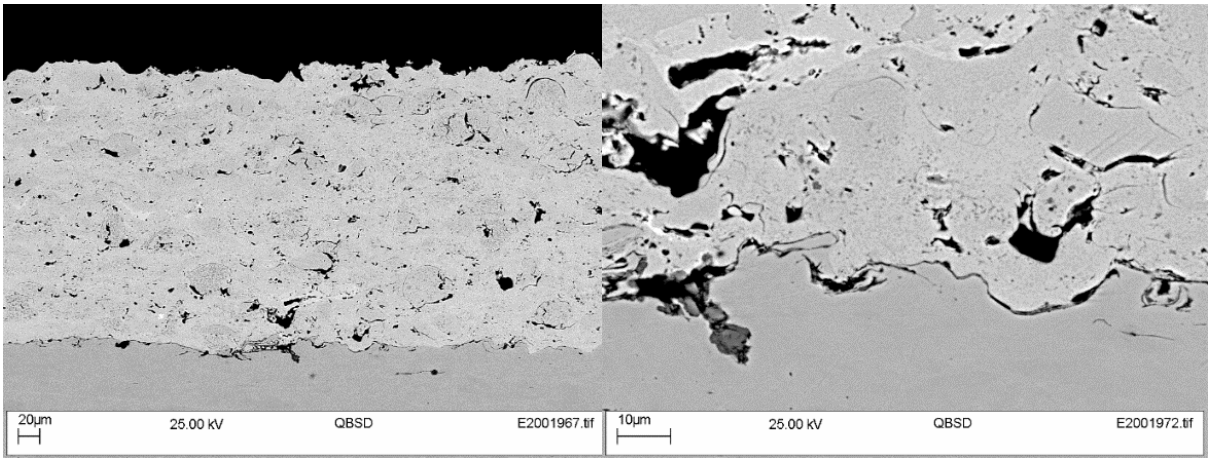

Figure 22 SEM micrographs of Coating 234Flux1 in back-scatter mode

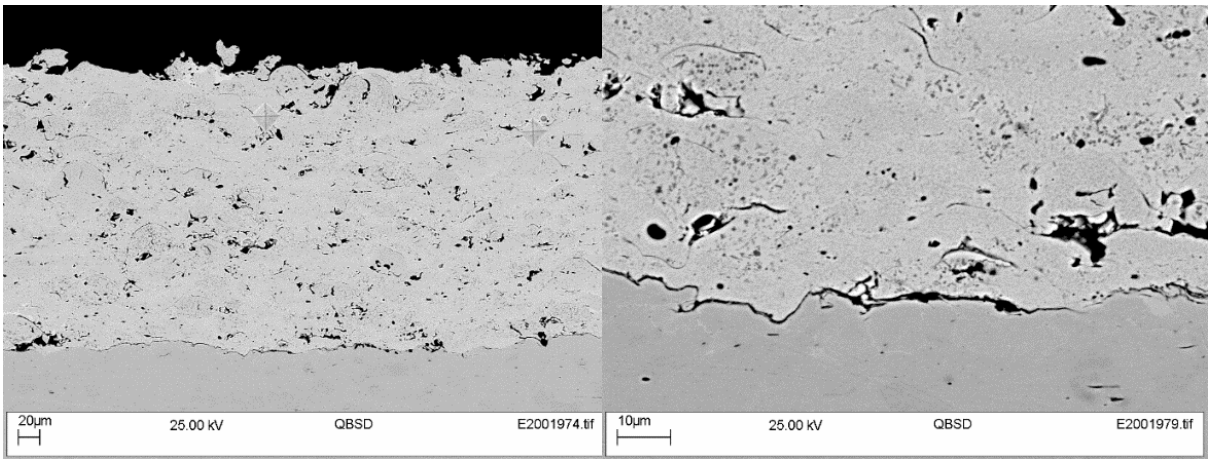

Figure 23 SEM micrographs of Coating 234Flux2 in back-scatter mode

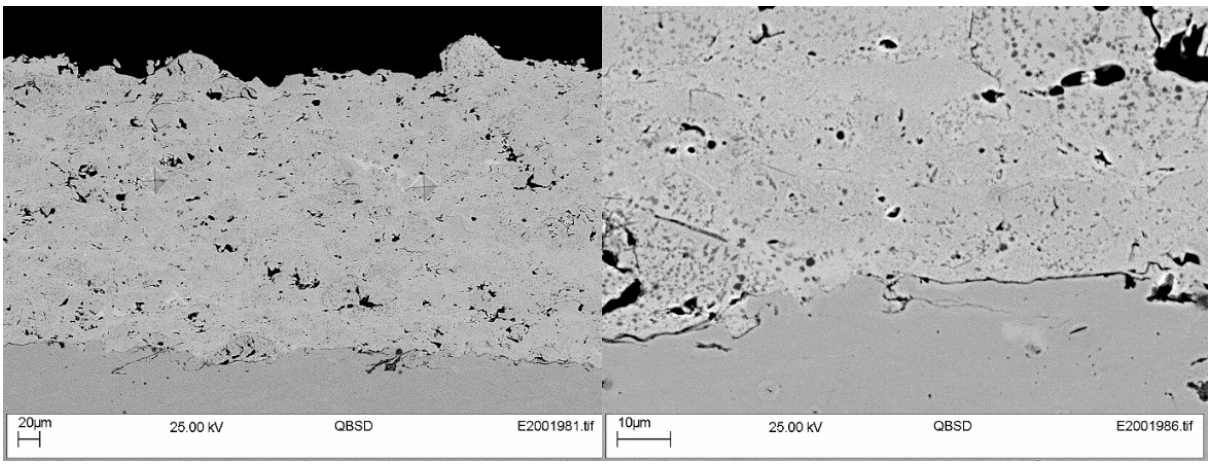

Figure 24 SEM micrographs of Coating 234Flux3 in back-scatter mode

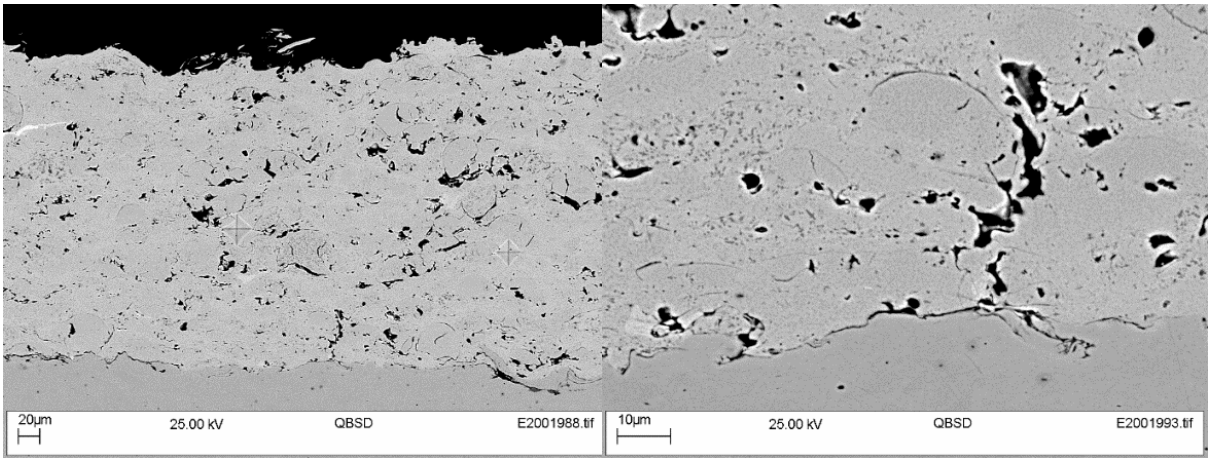

Figure 25 SEM micrographs of Coating 234Flux4 in back-scatter mode

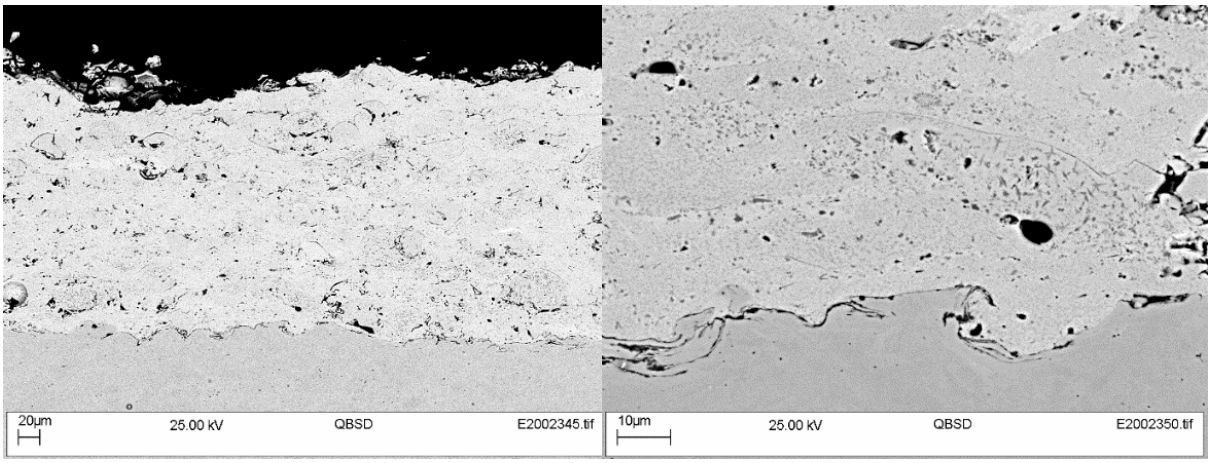

Figure 26 SEM micrographs of Coating 234Flux5 in back-scatter mode

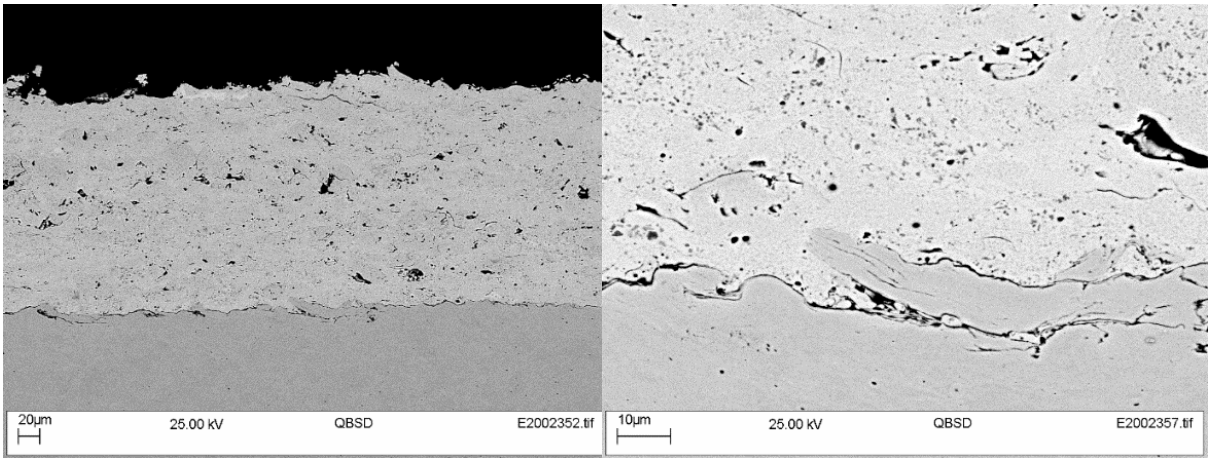

Figure 27 SEM micrographs of Coating 234Flux6 in back-scatter mode

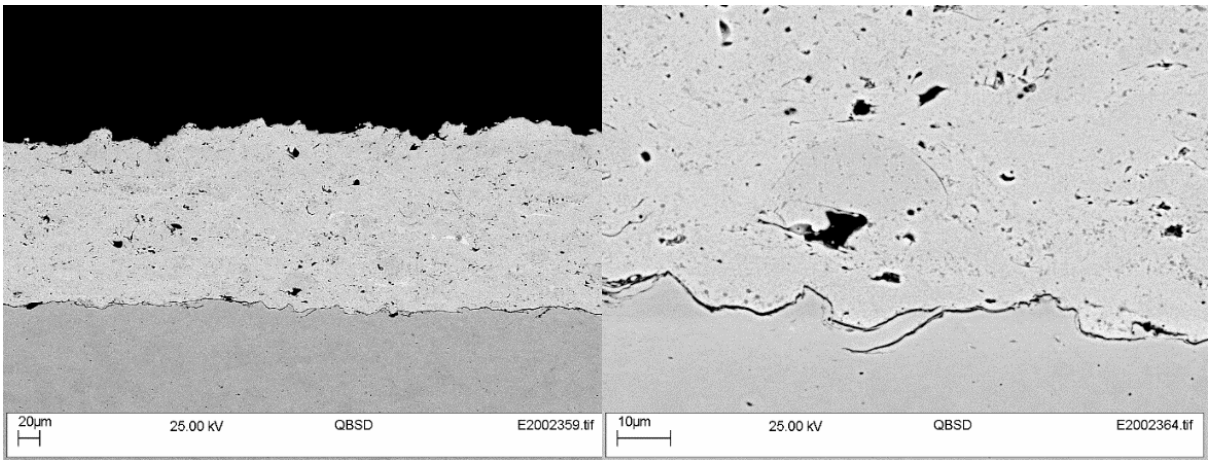

Figure 28 SEM micrographs of Coating 234Flux7 in back-scatter mode

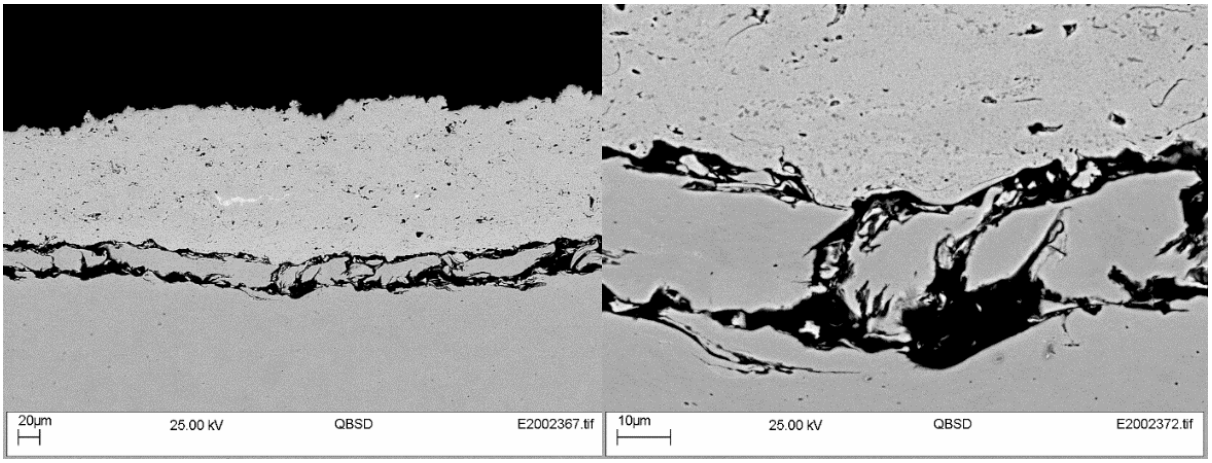

Figure 29 SEM micrographs of Coating 234Flux8 in back-scatter mode

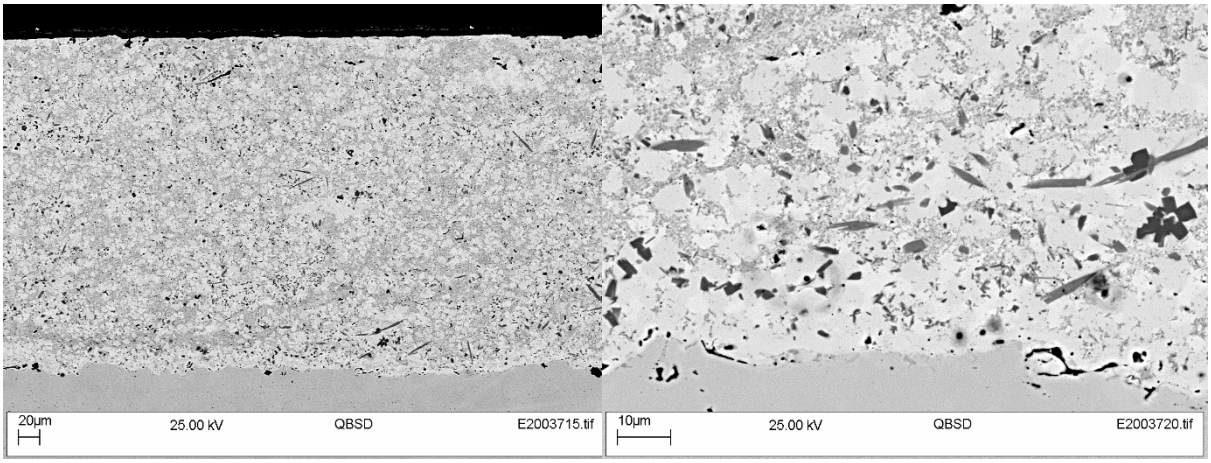

Figure 30 SEM micrographs of Coating 234Flux9-S in back-scatter mode

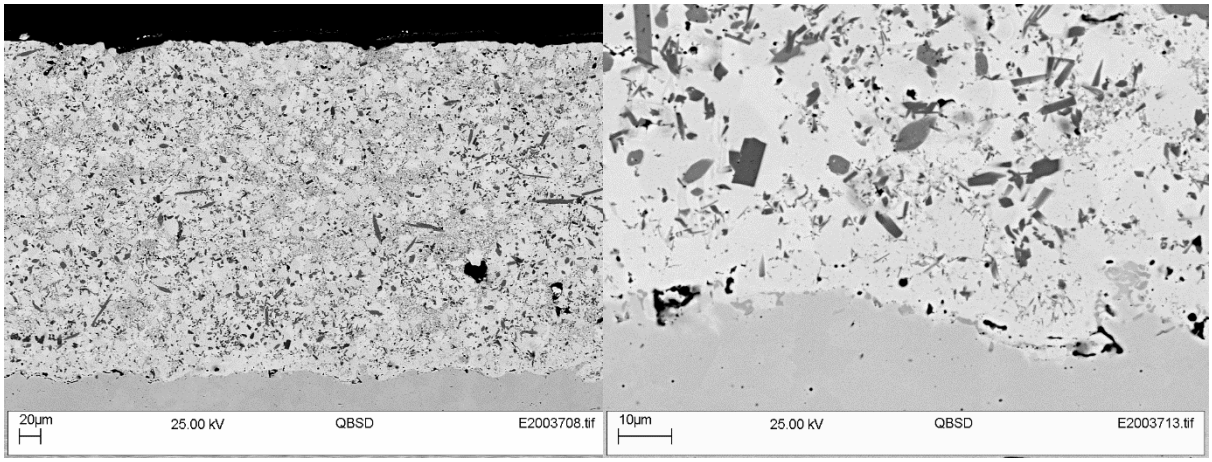

Figure 31 SEM micrographs of Coating 234Flux9-L in back-scatter mode

Table 16 Coating surface roughness of DoE matrix with NiCrFeSiB powder

Sample #	Oxygen flow, SLPM	Kerosene flow, SLPM	Spray distance, mm	Spray angle, °	Ra, µm		Rz, µm	
					Ave	Dev	Ave	Dev
234Flux1	897	0.385	380	90	5.8	0.3	41.3	2.3
234Flux2	930	0.350	380	90	6.0	0.4	37.2	1.8
234Flux3	930	0.385	380	90	6.4	0.4	39.5	3.3
234Flux4	897	0.350	380	90	6.9	0.3	41.7	2.3
234Flux5	930	0.385	350	90	6.9	0.6	42.9	2.8
234Flux6			380	70	5.4	0.5	34.6	2.4
234Flux7			380	50	4.6	0.3	28.8	0.7
234Flux8			380	30	5.9	0.3	35.0	1.7
234Flux9-S	930	0.385	380	90	1.2	0.2	16.1	5.5
234Flux9-L			380	90	1.9	0.4	20.0	6.0

Table 17 ASTM C633 adhesion testing results of NiCrFeSiB coatings

Run #	Oxygen flow, SLPM	Kerosene flow, SLPM	Spray distance, mm	Spray angle, °	Adhesion, MPa	
					Ave	Dev
234Flux1	897	0.385	380	90	34.6	3.2
234Flux2	930	0.350	380	90	37.9	3.5
234Flux3	930	0.385	380	90	38.6	4.9
234Flux4	897	0.350	380	90	43.1	3.3

Table 18 Test results of DoE matrix with NiCrFeSiB powders

Run #	Oxygen flow, SLPM	Kerosene flow, SLPM	Spray distance, mm	Spray angle, °	D.E., %	Porosity, %		Hardness, HV0.3	
						Ave	Dev	Ave	Dev
234Flux1	897	0.385	380	90	59	2.5	0.3	667	93
234Flux2	930	0.350	380	90	58	3.1	0.4	684	56
234Flux3	930	0.385	380	90	56	2.4	0.3	661	68
234Flux4	897	0.350	380	90	53	3.5	0.4	657	108
234Flux5	930	0.385	350	90	53	1.2	0.4	751	62
234Flux6			380	70	42	2.2	0.3	756	34
234Flux7			380	50	37	2.0	0.4	766	84
234Flux8			380	30	35	2.2	0.5	671	96
234Flux9-S	930	0.385	380	90		<0.2	-	863	53
234Flux9-L			380	90		<0.2	-	799	59

3.4 Nanocrystalline/amorphous coatings

3.4.1 Powder

SEM images of powder SHS 7574HV showed that the powder particles mainly have a spherical or oval shape (Figure 32). All these images were taken under back-scattered mode, and indicate that the powder was well alloyed and each elements was homogeneously distributed. Information received from the supplier shows that this powder is an eight- element Fe-Cr-Mo-W-Mn-B-C-Si material that was designed to have high glass forming ability. Its EDX spectrum shows the presence of Fe, Cr, C, Mo, Mn, W peaks. Boron (B) could not be detected in the spectrum either due to its low atomic number or its peak overlapping with other elements.

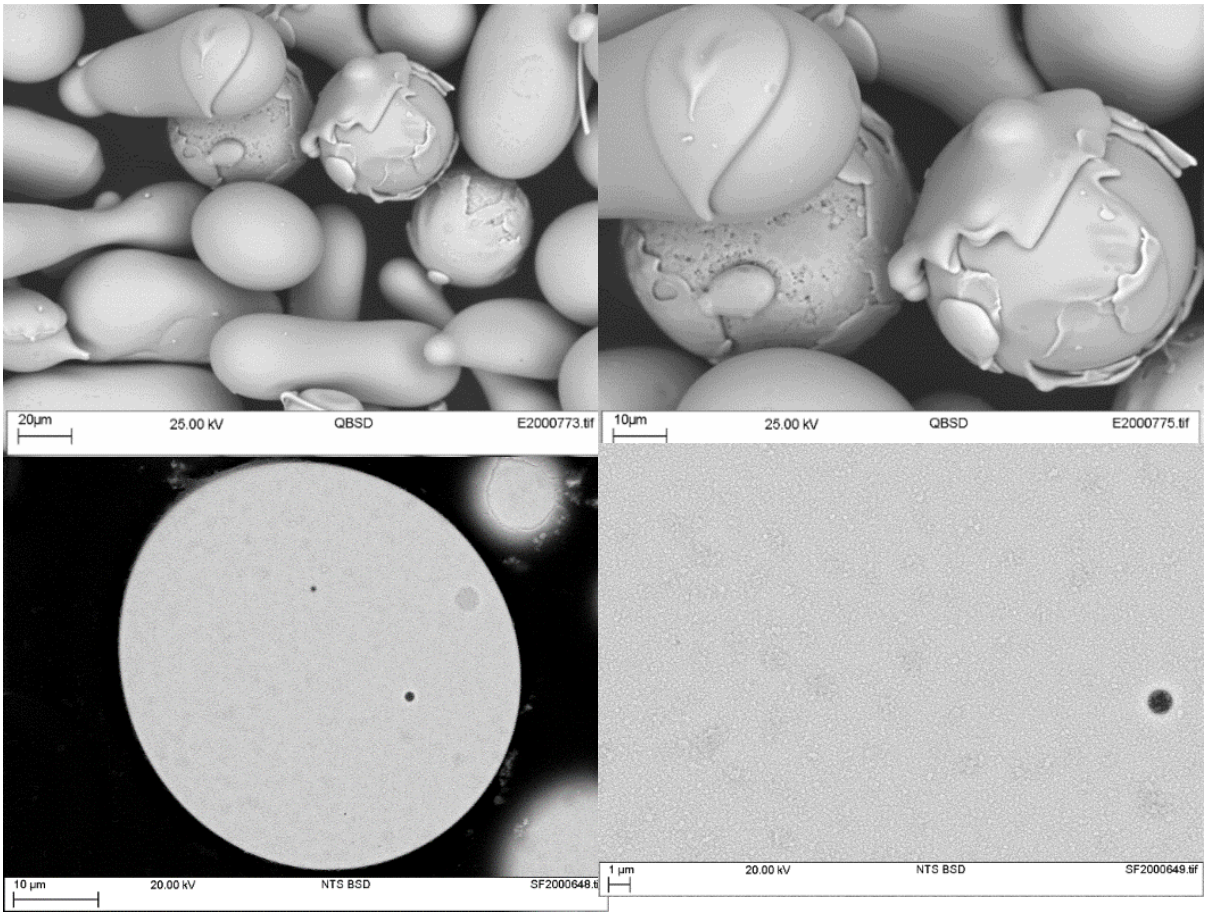

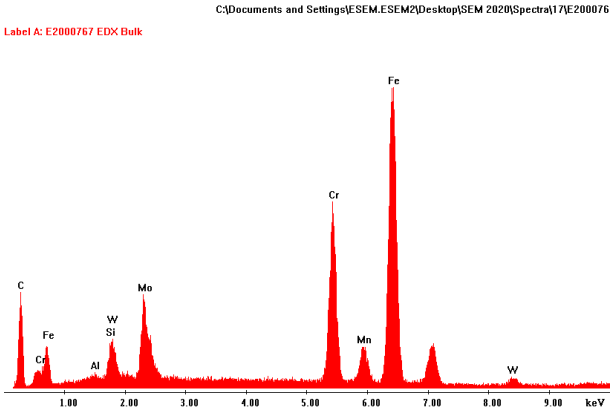

Figure 32 SEM and EDX analysis of as-received powder 4274, SHS 7574HV

3.4.2 Coatings

SEM images of nanocrystalline/amorphous coatings show that their microstructure presents a typical lamellar structure. However, their microstructure and properties vary a lot when deposited under different parameters (Figure 33-Figure 38, Table 19-Table 21):

- When kerosene flow decreases at fixed oxygen flow rate, it means a decrease in chamber pressure and temperature. Nanocrystalline/amorphous coatings (235Amor1 vs 235Amor2 vs 235Amor3, 235Amor4 vs 235Amor5) show an increase of surface roughness with Ra increassing from 7.5 to 8.9 µm and from 8.5 to 9.2µm for each group, respectively. Their porosity also increases from 2.6 to 8.8% and from 3.6 to 9.5% for each group, respectively. Moreover, more horizontal cracks are generated and the amount

of unmelted particles is also increased in the coating when the kerosene flow rate decreases. Correspondingly, their adhesion strength also decreases, from 43.2 to 25.6MPa for group 235Amor1 vs 235Amor2 vs 235Amor3 and from 34.5 to 25.3MPa for group 235Amor4 vs 235Amor5. This can be ascribed to poorer melting of powders due to lower combustion temperature and pressure when lower kerosene flow is being used while oxygen flow remains the same.

- When oxygen flow rate decreases at fixed fuel flow rate, it means an increase in the chamber pressure and a decrease of temperature. Nanocrystalline/amorphous coatings (235Amor2 vs 235Amor6 vs 235Amor4, 235Amor3 vs 235Amor5) show an increase of surface roughness with Ra increasing from 7.7 to 8.5 µm and from 8.9 to 9.2 µm, respectively. However, their porosity varies; the 235Amor4 coating presents the lowest density of 3.6%. Their hardness generally increases when oxygen flow rate decreases.
- X-ray diffraction analysis was carried out with one of the as-deposited nanocrystaline/amorphous coatings, 235Amor1, to study its crystalline structure, as shown in Figure 39. The broad amorphous peak and lack of distinct Bragg diffraction peaks suggest an amorphous structure and verifies that the as-sprayed coating's structure is primarily a metallic glass. Though metallic glass coatings can be subsequently heat-treated above their crystallisation temperature to cause the solid-state devitrification transformation to form nanocomposite coatings [12], this will not be covered in this project due to cost.

From the above, coating 235Amor4 was selected as the best, from the process parameters tested, due to its low porosity and high hardness.

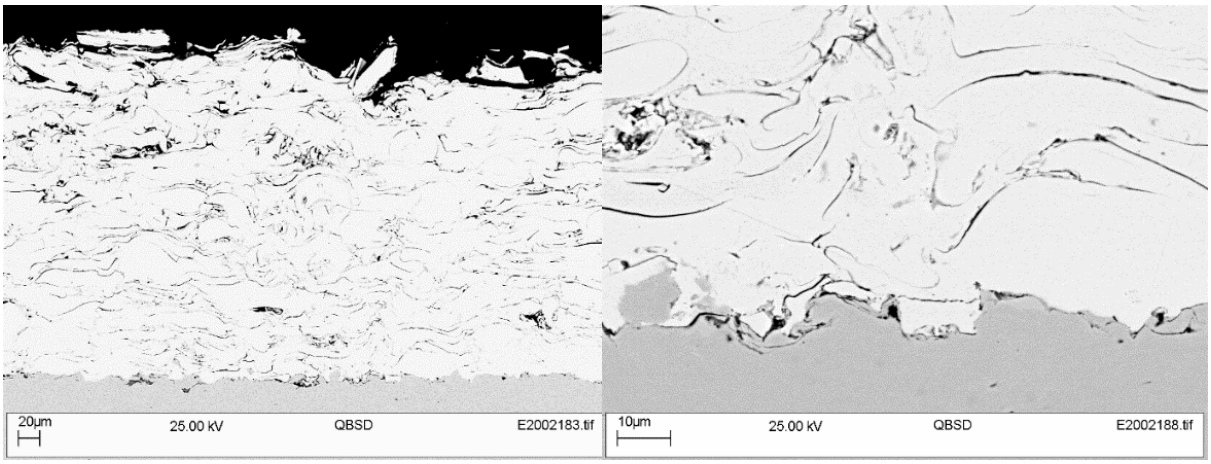

Figure 33 SEM micrographs of Coating 235Amor1 in back-scatter mode

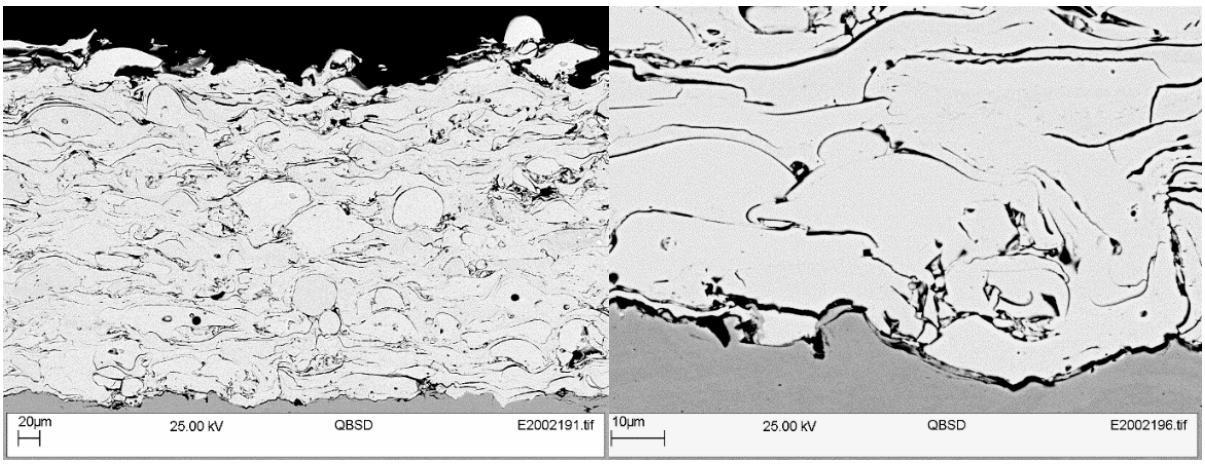

Figure 34 SEM micrographs of Coating 235Amor2 in back-scatter mode

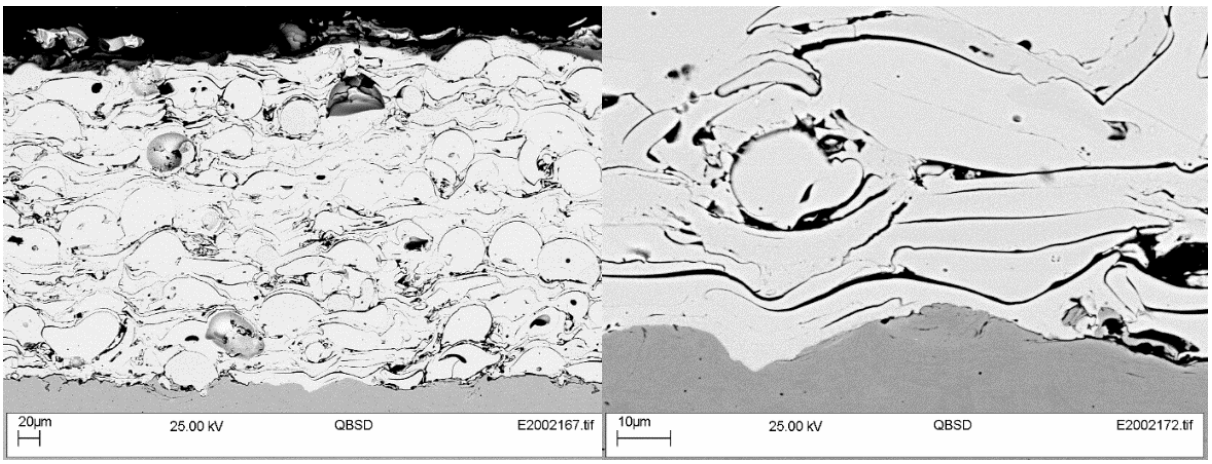

Figure 35 SEM micrographs of Coating 235Amor3 in back-scatter mode

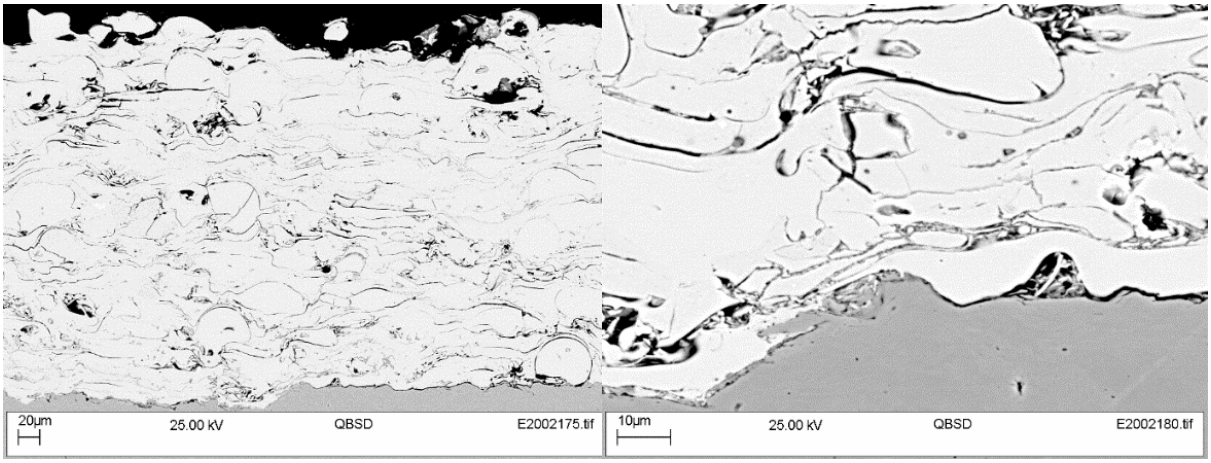

Figure 36 SEM micrographs of Coating 235Amor4 in back-scatter mode

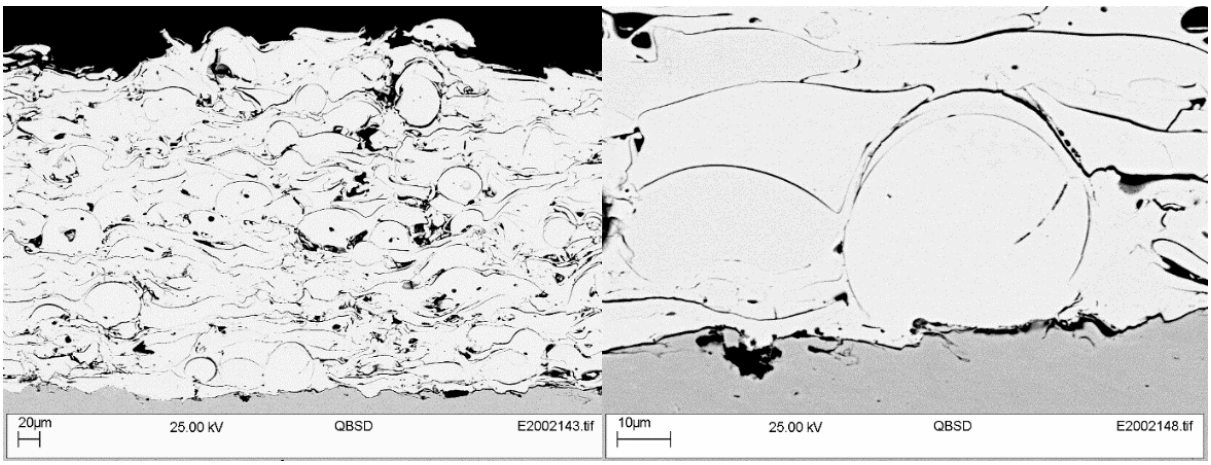

Figure 37 SEM micrographs of Coating 235Amor5 in back-scatter mode

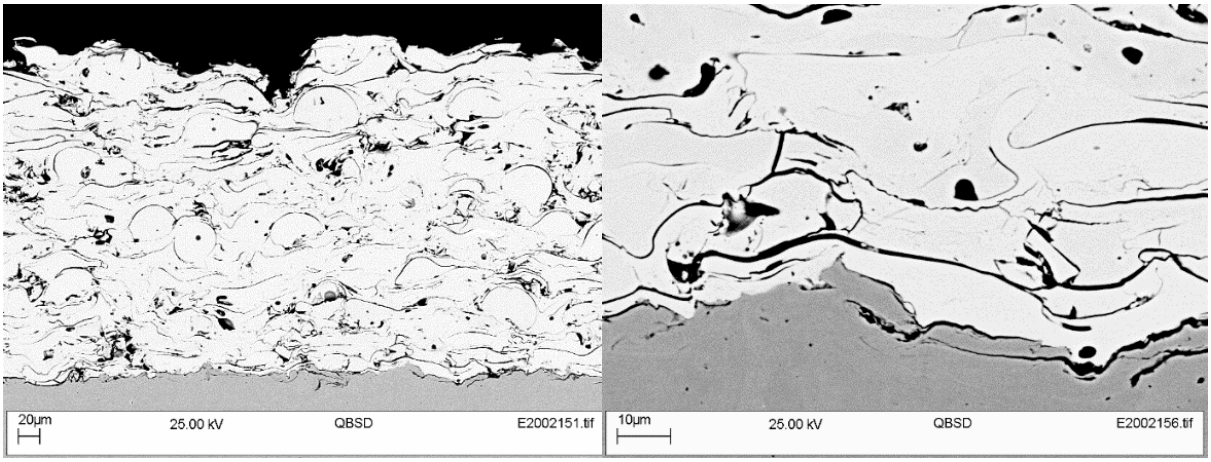

Figure 38 SEM micrographs of Coating 235Amor6 in back-scatter mode

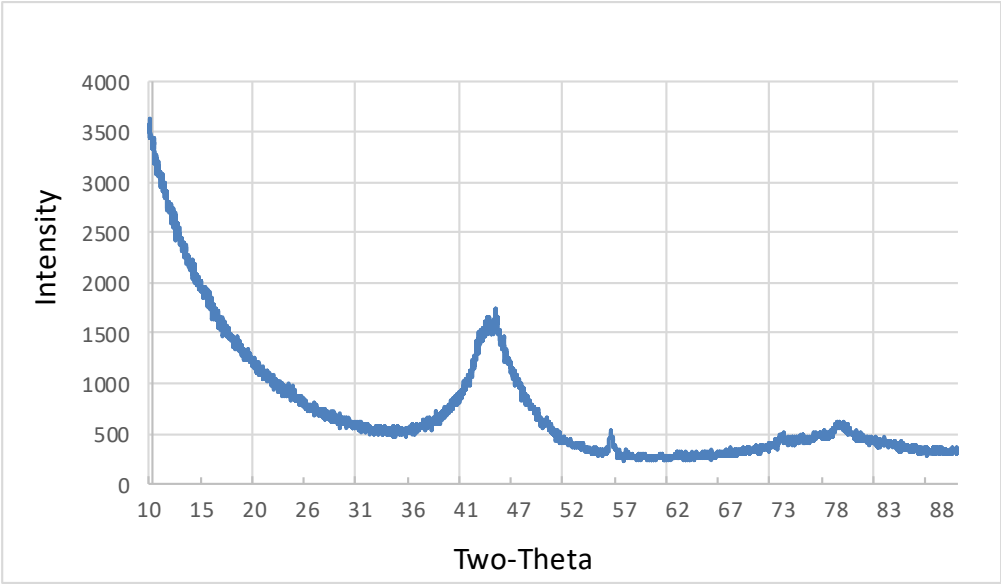

Figure 39 X-ray diffraction diagram of the as-sprayed amorphous HVOF coating 235Amor1

Table 19 As-deposited coating surface roughness of DoE matrix with amorphous/nanocrystalline powder

Run #	Oxygen flow, SLPM	Kerosene flow, SLPM	Ra, µm		Rz, µm	
			Ave	Dev	Ave	Dev
235Amor1	920	0.400	7.5	0.4	45.5	2.7
235Amor2	920	0.370	7.7	0.8	47.4	7.2
235Amor3	920	0.330	8.9	1.2	54.1	6.1
235Amor4	873	0.370	8.5	0.4	48.4	0.4
235Amor5	873	0.330	9.2	0.3	55.8	5.4
235Amor6	897	0.370	8.4	0.4	50.6	5.7

Table 20 Results of ASTM C633 adhesion testing of amorphous/nanocrystalline coatings

Run #	Oxygen flow, SLPM	Kerosene flow, SLPM	Adhesion, MPa	
			Ave	Dev
235Amor1	920	0.400	43.2	3.2
235Amor2	920	0.370	31.4	2.7
235Amor3	920	0.330	25.6	3.1
235Amor4	873	0.370	34.5	3.5
235Amor5	873	0.330	25.3	3.1
235Amor6	897	0.370	30.2	4.7

Table 21 Test results of DoE matrix with amorphous/nanocrystalline powders

Run #	Oxygen flow, SLPM	Kerosene flow, SLPM	Deposit efficiency, %	Porosity, %		Hardness, $HV_{0.3}$	
				Ave	Dev	Ave	Dev
235Amor1	920	0.400	44	2.6	0.8	660	108
235Amor2	920	0.370	45	5.5	0.7	752	127
235Amor3	920	0.330	44	8.8	1.1	730	201
235Amor4	873	0.370	46	3.6	0.7	827	122
235Amor5	873	0.330	45	9.5	2.2	765	159
235Amor6	897	0.370	45	7.9	1.1	815	133

4. PRODUCTION OF TEST SAMPLES

A number of test coupons have been produced for the first round of testing in WP3. The first round of test coupons for each material type includes 12 adhesion test coupons (both 34CrNiMo6 (EN24T) and 440B substrates, 6 off each), 5 slurry test coupons (34CrNiMo6 (EN24T) substrate), 5 wear-rotation test coupons (34CrNiMo6 (EN24T) substrate), 10 corrosion test coupons (34CrNiMo6 (EN24T) substrate), and 8 erosion-corrosion test coupons (34CrNiMo6 (EN24T) substrates).

Spray parameters and expected coating properties are summarised in Table 22. More test coupons will be prepared for further testing such as ring-on-ring, tribo-corrosion etc once results from the first round are released and discussed.

Table 22 Process parameters and expected properties for test coupons for first round of WP3 testing *

	WC-Co-Cr coatings	CrC-NiCr coatings	Self-fluxing Ni-based coatings	Fe-based amorphous coatings
ID	232WC	233CrC	234Flux	235Amor
Powder	Woka 3652 FC	1375VF	1660-02	SHS 7574HV
Powder TWI ID	4278	4277	4279	4274
Run conditions	232WC2	233CrC6	234Flux3	235Amor4
Spray angle, °	90	90	90	90
Powder carrier gas	Argon	Argon	Argon	Argon
Gun traverse speed, mm/s	900	900	900	900
Increment, mm	5	5	5	5
Specimen cooling	Air	Air	Air	Air
Nozzle	6 inch	6 inch	4 inch	4 inch
Powder feeder	Two-way	Three-way	Two-way	Two-way
Powder feed rate, rpm	350	200	150	200
Carrier gas flow rate, scfh	23	28	26	25
Spray distance, mm	350	350	380	350
Oxygen flow, SLPM	920	873	930	873
Kerosene flow, SLPM	0.400	0.340	0.385	0.340
Surface roughness (Ra), µm	4.3±0.5	3.5±0.7	6.4±0.4	8.5±0.4
Porosity, %	0.9±0.3	1.1±0.1	2.4±0.3	3.6±0.7
Hardness, $HV_{0.3}$	1218±112	755±72	661±68	827±122
Adhesion strength, MPa	-	73.9±10.3	38.6±4.9	34.5±3.5

Note: * coating characteristics are subject to being deposited on bright mild steel; they may vary if a different substrate material is used.

5. CONCLUSIONS

The four coatings with the best overall characteristics (from the process conditions tested) from each material type were selected to be tested in WP3 after the development of process parameters in this report. This includes:

- WC-Co-Cr coating, with average surface roughness of 4.3±0.5µm, porosity of 0.9±0.3%, and hardness of 1218±112$HV_{0.3}$.

- CrC-NiCr coating, with average surface roughness of 3.5±0.7µm, porosity of 1.1±0.1%, and hardness of 755±72$HV_{0.3}$.
- Self-fluxing Ni-based coating, with average surface roughness of 6.4±0.4µm, porosity of 2.4±0.3%, and hardness of 661±68$HV_{0.3}$.
- Fe-based amorphous coating, with average surface roughness of 8.5±0.4µm, porosity of 3.6±0.7%, and hardness of 827±122$HV_{0.3}$.

These coatings have been used to produce test coupons for the first round of testing in WP3. More test coupons will be prepared for further testing such as ring-on-ring, tribo-corrosion etc once results from the first round are released and discussed.

REFERENCES

[1] R Ahmed. Contact fatigue failure modes of HVOF coatings, Wear, 2002, 253(3–4): 473-487,

[2] A Wank, B Wielage, T Grud, et al. Characterisation of the particle jet of different HVOF guns by means of LDA, ITSC 2005, Basel, CH, 2-4 May 2005.

[3] M Oksa, E Turunen, T Suhonen, T Varis, S-P Hannula. Optimization and Characterization of High Velocity Oxy-fuel Sprayed Coatings: Techniques, Materials, and Applications. Coatings. 2011; 1(1):17-52.

[4] N A Ahmad, Z Kamdi, Z Mohamad, A S Omar, N. Abdul Latif and A. L. Mohd Tobi. Characterization of WC-10Ni HVOF Coating for Carbon Steel Blade. IOP Conference Series: Materials Science and Engineering, Volume 165, Colloquium of Advanced Mechanics (CAMS2016), Johor, Malaysia. 18–19 December 2016.

[5] M A Zavareh, A A D M Sarhan, B B Razak, W J Basirun, The tribological and electrochemical behavior of HVOF-sprayed Cr_3C_2–NiCr ceramic coating on carbon steel, Ceramics International, V2015, 41(4): 5387-5396.

[6] Y Shieh, J Wang, H C Shih, S Wu. Alloying and post-heat-treatment of thermal-sprayed coatings of self-fluxing alloys. Surface and Coatings Technology, 1993, 58(1): 73-77.

[7] M Cherigui, H.I Feraoun, N.E Feninehe, H Aourag, C Coddet, Structure of amorphous iron-based coatings processed by HVOF and APS thermally spraying. Materials Chemistry and Physics. 2004, 85(1): 113-119.

[8] N. Espallargas, J. Berget, J.M. Guilemany, A.V. Benedetti, P.H. Suegama. Cr_3C_2–NiCr and WC–Ni thermal spray coatings as alternatives to hard chromium for erosion–corrosion resistance. Surface and Coatings Technology.2008, 202(8): 1405-1417.

[9] A Surzhenkov, A Vallikivi, V Mikli, M Viljus, T Vilgo, P Kulu. Wear resistant self-fluxing alloy based tic-nimo and cr2c3-ni hardmetal particles reinforced composite coatings. The proceedings of the 2nd international scientific conference manufacturing engineering & management 2012, prešov, slovak republic, 2012.

[10] A Surzhenkov, M Antonov, V Mikli, J Latokartano, T Vilgo, P Kulu. Sliding wear of hvof sprayed self-fluxing alloy matrix cermet particles reinforced composite coatings. Conference: VII International Scientific Conference BALTTRIB 2013, Kaunas Lithuania. 2013

[11] M Giacomantonio, S Gulizia, M Jahedi, Y Wong, R Moore, M Valimberti. Heat treatment of thermally sprayed Ni-based wear and corrosion coatings. Materials Forum. 2011, 35: 48-55.

[12] D J Branagan, M C Marshall, B E Meacham, L F Aprigliano, R A Bayles, E J Lemieux, T M Wolejsza, F J Martin, D J J Haslam, S D Day, J C Farmer. Wear and Corrosion Resistant Amorphous/Nanostructured Steel Coatings For Replacement of Electrolytic Hard Chromium. Thermal Spray 2006: Proceedings of the International Thermal Spray Conference. Seattle, Washington, USA, May 15-18, 2006 .